Cool star winds and mass loss: Theory

Erwin Sedlmayr and Jan Martin Winters

Institut für Astronomie & Astrophysik, Technische Universität Berlin,
Sekr. PN 8-1, Hardenbergstr. 36, D-10623 Berlin, Germany
e-mail: Sedlmayr@physik.TU-Berlin.DE; Winters@physik.TU-Berlin.DE

Abstract. We describe the ingredients necessary for the consistent theoretical description of dust forming circumstellar shells around Red Giants on the asymptotic giant branch. The complete set of equations required for the reliable modeling of stationary and pulsating situations is discussed and applied to a dust driven wind and to a typical carbon rich Mira atmosphere. Special emphasis is put on the theoretical description of the dust formation process and on the complex interaction among dust formation, chemistry, hydrodynamics, thermodynamics and radiative transfer. We present some fundamental implications of a consistent description of the dust forming system on its observable appearance.

1 General Overview

All stars, except perhaps the most compact objects like White Dwarfs or neutron stars, exhibit a more or less pronounced mass loss proved by clear observed signatures like circumstellar reddening, extended shells, P–Cygni line profiles, radial velocity fields, etc. The mass loss rates $\dot{M}$ are strong functions of the object's position in the HR diagram and range from insignificant values ($\dot{M} < 10^{-12} M_{\odot}\mathrm{yr}^{-1}$) characterizing objects at the lower main sequence up to huge values ($\dot{M} = 10^{-6} - 10^{-4} M_{\odot}\mathrm{yr}^{-1}$) for objects in the upper region of the HR diagram, i.e. those objects having extremely high luminosities (see Fig. 1).

A detailed inspection of the stellar mass loss phenomenon reveals different modes of mass loss being connected with the various types of objects in the HR diagram (see Fig. 2):

i) *quasi stationary winds:* These are observed in hot O and B stars, in solar type objects and in K giants, where the mass loss phenomenon seems to be a long lasting process with typical time scales larger than 10^5yr.

ii) *periodic and semi regular mass loss:* In these cases, which are observed in the outflows of Miras and long–period variable stars (LPVs), the mass loss shows a distinct periodic variation which is believed to be connected with the intrinsic stellar pulsations and seems to be triggered by outwards traveling shock waves generated at the bottom of the stellar atmosphere.

iii) *episodic mass loss:* This mode is observed in RCrB–type stars, Wolf–Rayet stars and of course in explosive events like novae and supernovae.

Despite this rather complex observational situation there seems to be a rather systematic distinction between the various driving mechanisms for the

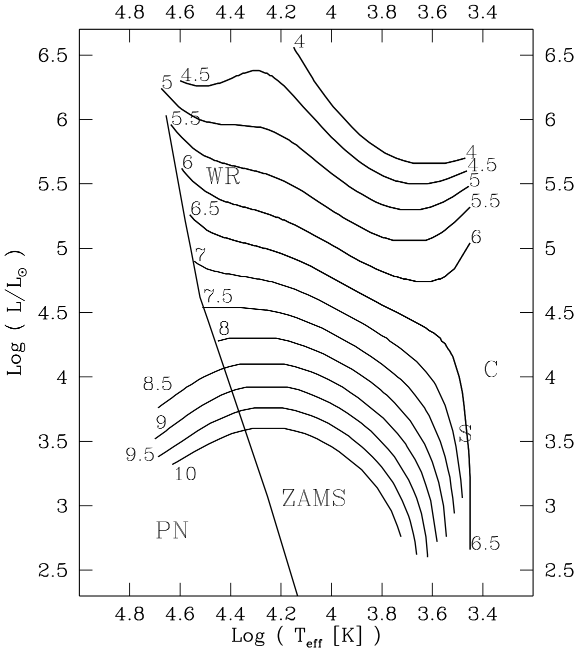

Fig. 1. Lines of constant mass loss rate in the HR diagram (after de Jager et al. 1988). Labels are $-\log_{10}(\dot{M})$

quasi–stationary	hot stars, K giants	ζ Pup, ζ Aur
(quasi)periodic	Miras, semi–regular Variables	o Cet, RScl
episodic	RCrB, Wolf–Rayet stars, SN, Novae	RCrB, WR140, SN1987a, V846Cen

Fig. 2. The different modes of mass loss, respective class of objects, and representative objects

mass loss as depicted in Fig. 3. There are only two basically different mechanisms: radiation induced (being addicted to high luminosity objects) and wave induced winds (being addicted to objects generating considerable wave energy near the surface of the star), respectively. As most giants and supergiants show a more or less pronounced variability, radiative acceleration of the wind might not be the only driving mechanism, but also momentum and energy input by waves should contribute to or even dominate the generation of the wind and consequently the radial structure of the velocity field. Therefore, a simultaneous treatment of radiative momentum transfer to the matter and momentum and energy dissipation in the wave field is required to model the mass loss phenomenon in these cases.

Since the lecture of H. Lamers reviews the general aspects and the basic

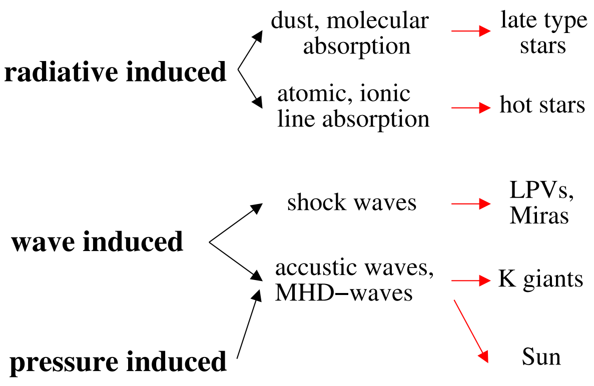

Fig. 3. Basic driving mechanisms

theoretical concepts of stellar winds throughout the HR diagram, in this lecture we will focus on the mass loss of late type stars, in particular of AGB objects, where mass loss plays a central role not only for the understanding of their shell structure but also for the evolution of the object itself.

2 Basic characteristics of late type stars

2.1 HR diagram characteristics

Red giants and supergiants are evolved objects occupying the upper right part of the HR diagram. These objects are characterized by rather cool (red!), extended (giant!) shells having low expansion velocities but rather large mass loss rates. A compilation of some important characteristic properties of these AGB objects is given in Tab. 1.

Table 1. Characteristic quantities of dust forming late type stars

stellar mass	$M_\star$	$\sim 0.7 \ldots 2.0\,M_\odot$
stellar luminosity	$L_\star$	$\sim 10^3 \ldots 10^5\,\mathrm{L}_\odot$
stellar temperature	$T_\star$	$\sim 2000 \ldots 3000\,\mathrm{K}$
mass loss rate	$\dot{M}$	$10^{-7} \ldots 10^{-4}\,M_\odot\mathrm{yr}^{-1}$
wind velocity	v_∞	$\sim 10 \ldots 30\,\mathrm{km\,s}^{-1}$
mass of the shells	M_{CS}	$\sim 0.1 \ldots 0.6\,M_\odot$
pulsation period	P	$\sim 100 \ldots 1000\,\mathrm{d}$

An important signature is the observation of significant dust formation causing pronounced reddening and, in extreme cases, complete obscuration of the central stars. Though most objects in this region of the HR diagram are due to their evolutionary state intrinsic variables like Miras and LPVs – which clearly can be found in the detailed temporal and spatial signatures of the wind – the stellar mass loss phenomenon itself in most cases seems to be a long–lasting process whose secular variations are finally controlled by the intrinsic evolutionary time scale of the star.

In all objects the occurrence of dust seems to have a decisive impact upon the detailed shell structure, the local dynamics, and finally upon the overall appearance of the object as manifested e.g. by a clear correlation between the observed stellar mass loss rate and the circumstellar dust abundance measured by the IRAS colors which is found for many late type stars (cf. Fig. 4). A second important fact is that the observed high mass loss rates are carried by rather low expansion velocities drawing a clear distinction to hot star winds where similar high mass loss rates always are connected with expansion velocities being at least a factor of 100 larger. The low expansion velocity and high mass loss rate, together with the fact, that the objects under consideration only have low surface gravity, places important constraints on the mass loss mechanism: Most of the energy transfered to the wind must be deposited in the sub-sonic (inner) region to account for the observed high mass loss rate. Only a small fraction of the driving energy can be supplied in the supersonic (outer) wind regime in order to accelerate the wind to its low terminal velocity. For a detailed discussion of the basic physical constraints imposed on the driving mechanism of the wind, we refer to the excellent review of Holzer & MacGregor (1985).

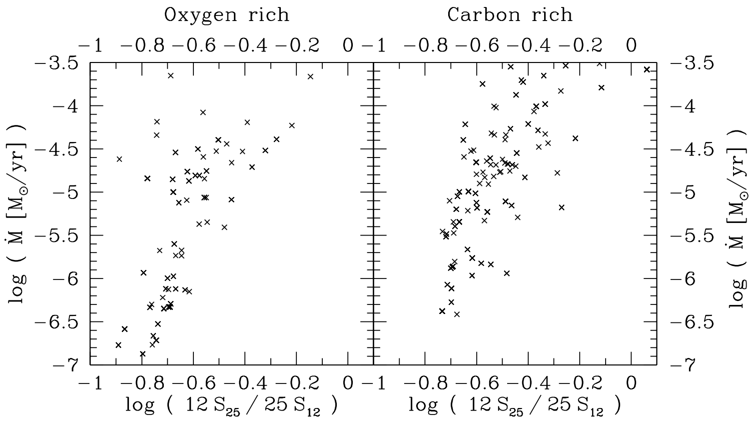

Fig. 4. Correlation between mass loss rate and IRAS colors (from Loup et al. 1993)

2.2 Shell characteristics

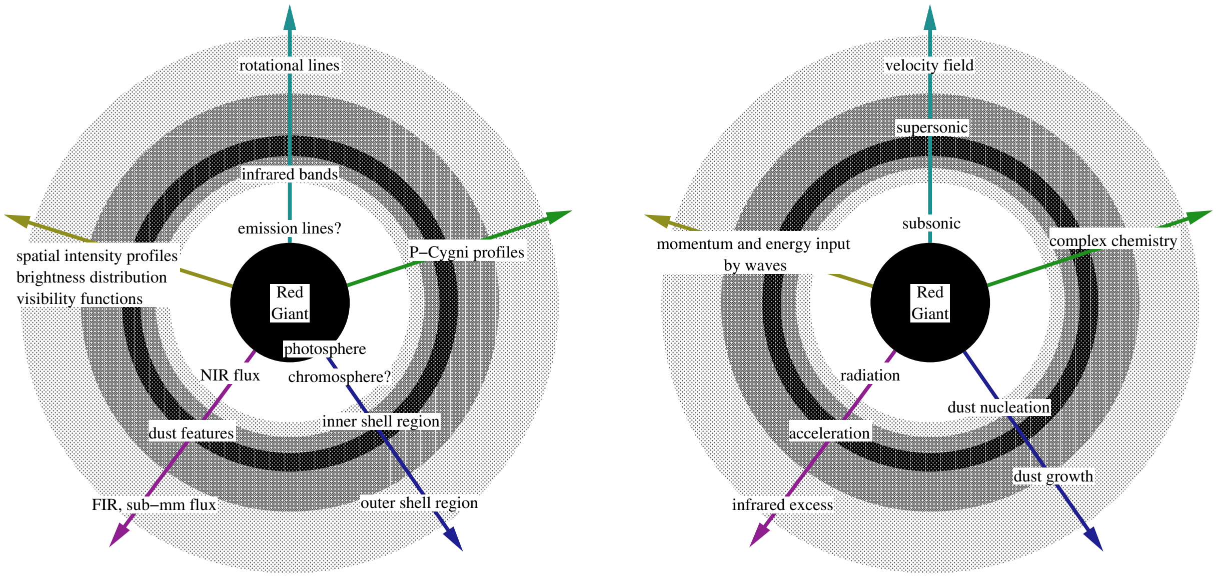

Fig. 5. Observed appearance and physical mechanisms in a typical circumstellar dust shell

For a typical Red Giant, Fig. 5 depicts both, the observational side and the theoretical side of the problem by focusing various distinct features of the observational appearance as well as important processes constituting necessary ingredients of the theoretical description which are required for a reliable physical understanding of such objects.

Observational facts: The spectra of the objects show P Cygni line profiles, being a clear signature of the shell expansion caused by a stellar wind. Typical expansion velocities range from $10\ldots30\,\mathrm{km\,s^{-1}}$ thus being extremely supersonic. The P Cyg profiles are found in a variety of molecular lines (e.g. Keady & Ridgway 1993) demonstrating the radial evolution of both, the complex chemistry and the increasing velocity. From a detailed modeling of these infrared molecular lines the radial density distribution and the mass loss rate can be inferred. In almost all AGB objects, also rotational emission lines of various molecules originating in the outer region of the shells are observed at radio wavelengths, from which usually the terminal wind velocity and the mass loss rates in the outer shell regions are derived (e.g. Knapp & Morris 1985).

A noticeable feature observed in nearly all objects in this region of the HR diagram is effective dust formation in the cooling outflow which manifests itself by a significant reddening of the continuum radiation field, large infra–red (IR) excesses and specifically by pronounced dust absorption or emission bands. In some objects, in particular early M giants, also emission lines are observed in the UV and visual spectral region, indicating a non–monotonic temperature structure which usually is attributed to the existence of a chromosphere well inside the dust forming region.

High spatial resolution observations in different wavelength bands reveal a rather complex radial structure of the circumstellar dust shell (e.g. Ridgway & Keady 1988, Danchi et al. 1994). From such observations, the approximate location of the dust formation region can be inferred.

Physical processes: The basic feature of a red giant shell is the presence of a velocity field starting in the photosphere and showing a distinct subsonic–supersonic transition. This velocity field causes a cooling flow along which a more and more complex chemistry evolves providing beyond some radius (below 1300K) favorable conditions for cluster nucleation and grain growth. Due to its huge extinction coefficient, the dust grains very efficiently absorb radiation momentum and energy, which leads to an effective acceleration of the circumstellar material and to a pronounced infrared excess (see next section). Additional energy and momentum input to the material by wave dissipation causes a levitation of the atmosphere in the inner region and, in connection with the effects introduced by the dust, might lead to severe influences on the radial structure of the dust shell (see Sect. 4.4).

3 Self-consistent description of dust forming circumstellar shells

The presence of dust in general has three severe impacts upon the thermodynamic, hydrodynamic, and chemical structure of the dust forming system:

i) Due to its specific absorption properties, dust grains – being macroscopic particles – dominantly absorb high energy photons and re-emit in the infrared regime, thus transforming the trapped short wavelength photons into long wavelength photons, for which the systems usually are transparent. Therefore the dust grains act as an energy sink in the equation of energy by channeling the energy out of the system.

ii) Due to its large absorption and scattering cross sections, the momentum of the radiation field is very effectively taken up by the dust grains and subsequently is transfered to the ambient gas by frictional coupling, thus causing an efficient radiative acceleration of the matter.

iii) By formation of macroscopic dust particles the chemistry is affected with regard to two aspects:

– By the dust formation process itself, causing a significant depletion of the chemical species involved in the formation of grains.

– By the formation of grains, surfaces are introduced into the system, which now are available for a variety of chemical reactions (like H_2 formation from atomic hydrogen) to take place which usually would not occur in the gas phase.

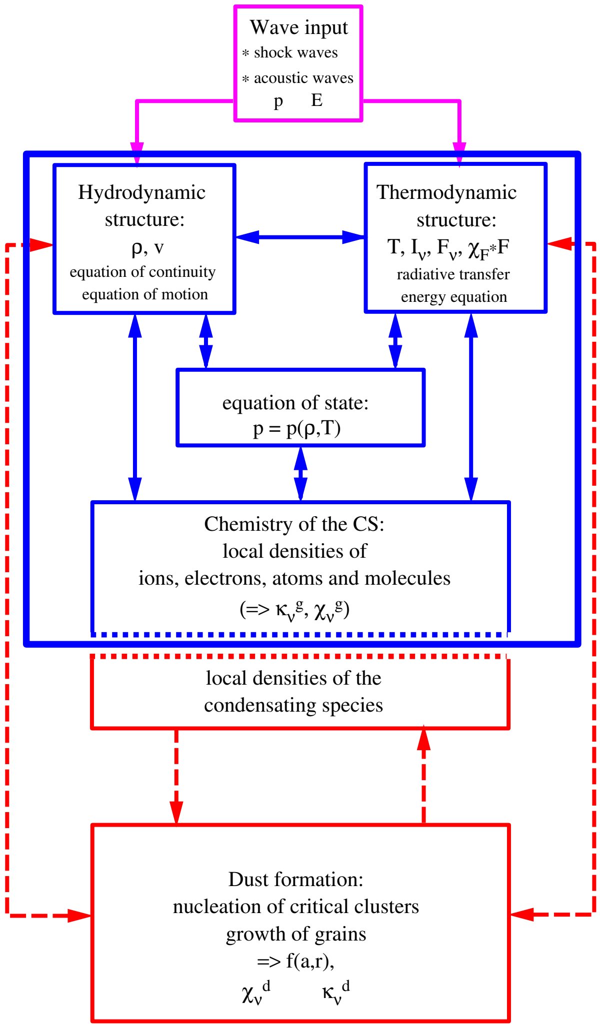

Fig. 6. Coupling among the different physical processes. The large box comprises the classical problem of a stellar atmosphere (after Sedlmayr & Winters 1991)

Due to these significant impacts of the grains on any dust forming system, also for the consistent description of a dust forming AGB star shell these aspects are of particular importance providing a close coupling among the chemical, thermodynamic, and hydrodynamic structure of the dust forming circumstellar shell (see Fig. 6). In the numerical modeling, these different processes, which are described in the following, have to be treated simultaneously, taking into account their mutual interactions.

3.1 Chemistry of the circumstellar shell

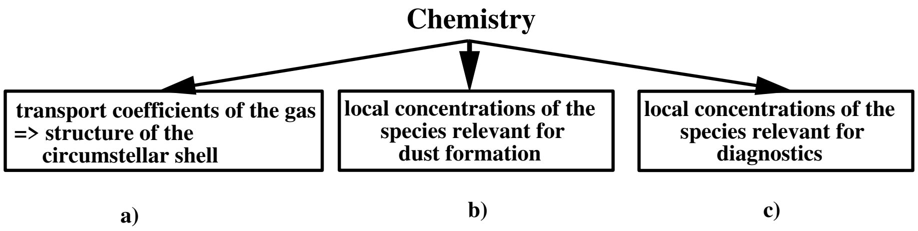

Fig. 7. General role of chemistry for a dust forming circumstellar shell

Figure 7 shows, that chemistry plays a central role with regard to three important aspects for the physical behavior of circumstellar shells which have to be considered in the quantitative modeling:

a) The chemical structure of the atmosphere and the shell i.e. the knowledge of the local concentrations of the various ionic, atomic and molecular species, determines the transport coefficients of the gas, which are most important ingredients for the quantitative thermodynamic and hydrodynamic modeling. This concerns in particular the molecular opacity coefficients which in two ways influence the model structure: i) atomic and molecular absorption and emission determine the radiative transfer and hence determine via the energy equation the local temperature of the system, and ii) the extinction coefficient determines the absorption of radiative momentum in particular in the molecular lines which in the equation of motion might contribute significantly to the outward directed acceleration causing possibly a levitation of the atmosphere (e.g. Jørgensen et al. 1992). As this effect introduces a pronounced increase of the scale height of the system, this is of particular importance for hydrostatic models, which might become sufficiently extended for further effective molecule formation and even dust formation to take place.

To get reliable molecular extinction, absorption and emission coefficients is by no means a simple problem since it requires both, realistic local molecular concentrations (see Sect. 3.1.1) and reliable monochromatic molecular transport coefficients per particle where a huge number of transitions usually has to be taken into account. For this purpose, either direct methods are applied by taking into account millions of individual lines in the transfer calculations or statistical approaches like the use of opacity distribution functions (ODF) or opacity sampling methods (OS), where for each frequency interval suitable average values accounting for the total contribution of the corresponding transitions are constructed. For further reading see the excellent reviews of Tsuji (1986) and Gustafsson (1989) and the recent conference proceedings on molecules in the stellar environment (Jørgensen 1994).

b) A second important aspect of the chemistry is that it provides the concentrations of the species being able to condense and thus provides the prerequisites for primary dust nucleation and growth. As the species relevant for dust formation usually are different from those molecules determining the basic atmospheric structure (see a)) their determination requires particular arguments being provided by both, the special nature of the observed circumstellar dust components, and the individual chemical behavior of the molecules under consideration. This complex is discussed in Sect. 3.2.

c) Finally, chemistry plays a central role with regard to a reliable interpretation of actual observations of circumstellar shells aiming at a quantitative diagnostics for real objects. Any detailed quantitative analysis has to be based on the knowledge of the local concentrations of the various species and therefore involves the detailed investigation and modeling of the chemical shell structure. From Fig. 6 one infers that this structure is strongly coupled with the various other boxes, thus clearly demonstrating that any reliable quantitative diagnostics of circumstellar shells has to be based on self-consistent theoretical descriptions.

3.1.1 Level of approach In all model calculations the chemistry turns out to be a most time consuming part of the necessary numerics. For this reason, any qualified judgment which allows to reduce the complexity of the problem to a still realistic minimum level is very useful. The necessary level of approach can be inferred from comparing the different time scales describing the various processes in a chemical network. This network consists of a set of continuity equations

$$\frac{\partial n_{\rm i}}{\partial t} + {\rm div}(\mathbf{v}\cdot n_{\rm i}) = \sum_{j=1}^{N}(Q_{\rm i,j}^{\rm c,g} - Q_{\rm i,j}^{\rm c,l}) + \sum_{j=1}^{N}(Q_{\rm i,j}^{\rm p,g} - Q_{\rm i,j}^{\rm p,l}) \tag{1}$$

where c denotes kinetic reactions, p denotes photo reactions, g and l are the gain and loss terms, respectively, $n_{\rm i}$ is the number density of species i, and N is the number of species considered in the network. For spherical symmetry, the divergence term is given by

$$ {\rm div}(\mathbf{v}\cdot n_{\rm i}) = \frac{1}{r^2}\frac{\partial}{\partial r}(r^2\, v\, n_{\rm i}) = v\frac{\partial n_{\rm i}}{\partial r} + \frac{2\,v}{r}\,n_{\rm i} + \frac{\partial v}{\partial r}\,n_{\rm i} \ \ ,$$

and the time evolution of $n_{\rm i}$ in co–moving coordinates is

$$\dot{n}_{\rm i} = \frac{dn_{\rm i}}{dt} = \frac{\partial n_{\rm i}}{\partial t} + v\frac{\partial n_{\rm i}}{\partial r} \ \ .$$

Inserting these expressions into Eq. (1) and dividing by the density n_i provides the respective time scales defined in Tab. 2 where the different states of equilibrium – which in principle may be encountered in a circumstellar environment – are depicted.

Table 2. Definition of the different time scales and different states of equilibrium. Definition: $\underbrace{ab\ldots} = min\{a, b, \ldots\} \gg |a + b + \ldots|$. Terms marked by "<<" can be neglected against the terms inside the braces. CE: chemical equilibrium, KE kinetic equilibrium (adopted from Goeres et al. 1988)

hydrodynamics			source terms		
$\frac{\dot{n}_\mathrm{i}}{n_\mathrm{i}}$	$2\,\frac{v}{r}$	$\frac{\partial v}{\partial r}$	$\frac{1}{n_\mathrm{i}}\sum_j \left(Q^{\mathrm{c,g}}_{\mathrm{i,j}} - Q^{\mathrm{c,l}}_{\mathrm{i,j}}\right)$	$\frac{1}{n_\mathrm{i}}\sum_j \left(Q^{\mathrm{p,g}}_{\mathrm{i,j}} - Q^{\mathrm{p,l}}_{\mathrm{i,j}}\right)$	
$\ll$	$\ll$	$\ll$	$\underbrace{\qquad\qquad}$	$\ll\quad\ll$	CE ($\rightarrow$ LTE)
$\underbrace{\qquad}$	$\underbrace{\qquad}$	$\underbrace{\qquad}$	$\underbrace{\qquad\qquad}$	$\ll\quad\ll$	CE ($\rightarrow$ LTE)
$\ll$	$\ll$	$\ll$	$\underbrace{\qquad\qquad}$	$\underbrace{\qquad\qquad}$	KE ($\rightarrow$ non LTE)
$\underbrace{\qquad}$	$\underbrace{\qquad}$	$\underbrace{\qquad}$	$\underbrace{\qquad\qquad}$	$\underbrace{\qquad\qquad}$	KE ($\rightarrow$ non LTE)
$\underbrace{\qquad}$	$\underbrace{\qquad}$	$\underbrace{\qquad}$	$\underbrace{\qquad\qquad}$	$\ll\quad\ll$	non CE
$\underbrace{\qquad}$	$\underbrace{\qquad}$	$\underbrace{\qquad}$	$\underbrace{\qquad\qquad}$	$\underbrace{\qquad\qquad}$	non KE
$\underbrace{\qquad}$	$\underbrace{\qquad}$	$\underbrace{\qquad}$	$\ll\quad\ll$	$\ll\quad\ll$	frozen chemistry
τ^{-1}_dil		τ^{-1}_acc	τ^{-1}_ch	τ^{-1}_ph	time scales
			$\tau^{-1}_\mathrm{source}$	$\tau^{-1}_\mathrm{source}$	

In a real circumstellar shell various chemical processes take place, which in their full complexity are depicted in Fig. 8. Though being impressively complicated, in many situations the description of the chemistry may be considerably simplified. Figure 9 shows various situations of circumstellar shells and the corresponding required approximations for the applied chemical network. As a general finding it may be stated that in the region beyond the sonic point, where the wind expands at a supersonic velocity, in any case a non–KE approach should be applied whereas for the inner region depending whether

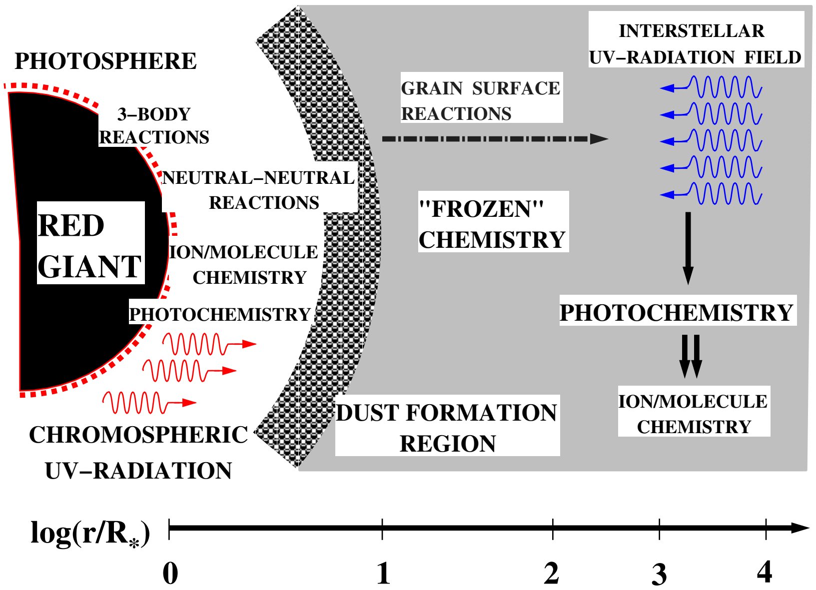

Fig. 8. Chemical processes in different regions of the circumstellar shells around red giants (adopted from Patzer et al. (1996a))

ionizing or dissociating photons are present or not, a CE or KE description might be appropriate. In situations, where shock waves are propagating through the system, always a non–KE approach has to be applied, even near the stellar surface. The chemical network equations basically have the form of an equation of continuity i.e. the l.h.s. consists of a partial time derivative of the concentration of the considered species and a divergence term applied to the corresponding flux density. This system of rate equations usually is applied to a co-moving mass element where the rate equations simply reduce to a system of first order nonlinearly coupled ordinary differential equations. Due to the huge range in magnitude of the different time scales governing the various reactions contributing to the network, in most applications the rate network turns out to be a stiff system requiring especially designed codes for a stable and sufficiently accurate solution. Being of first order in time, any solution of the chemical network requires the prescription of a suitable initial condition for the species under consideration. For a stellar wind which due to its expansion can be considered as a basically monotonic situation usually an initial condition is chosen provided by the chemical composition at the base of the photosphere where the temperature is large enough for all molecules to be completely dissociated. In many cases it is also appropriate to start with the calculations at a layer being sufficiently dense for chemical equilibrium to hold.

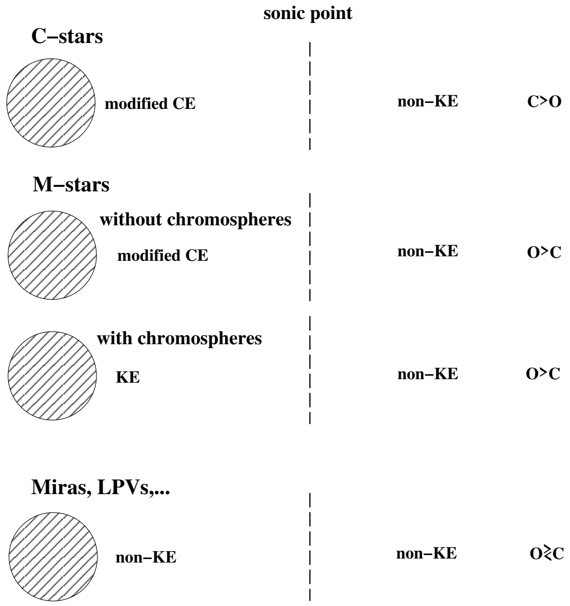

Fig. 9. Expected equilibrium situations with respect to the chemistry for different types of late–type stars

In order to demonstrate the effects of a non–KE situation compared to a chemical equilibrium calculation, in Fig. 10 the radial course of important molecules is shown for the inner and outer region of a shell model for the prominent carbon–rich infrared object IRC +10216. One clearly sees that the non–LTE effect generally does not influence the key molecules (H_2, CO, N_2) but obviously has a significant influence upon the reactive molecules (H, C_2H_2, HCN, C_2H, C, CN). Thus, even in the inner region of this C-rich wind CE does not hold but, due to the rapid expansion in the acceleration region a frozen chemistry develops. The external regions of a shell are always affected by two important processes, both increasing a departure from CE: i) Because of the rapid dilution in the supersonic wind, most reactions freeze out at some non equilibrium value (i.e. the corresponding reaction rate becomes negligible) and ii) due to the strong, high energetic interstellar UV field dissociating and ionizing photo reactions begin to influence the circumstellar wind from outside causing a rapid drop of the molecule abundances and the corresponding atoms and ions to show up.

3.1.2 The key role of the CO molecule Due to its extremely high bond energy (11.09 eV), the CO molecule plays a most important role for the kind of chemistry to be expected in a circumstellar shell. Considering a mass element moving outwards along the expansion trajectory of the stellar wind, CO is the

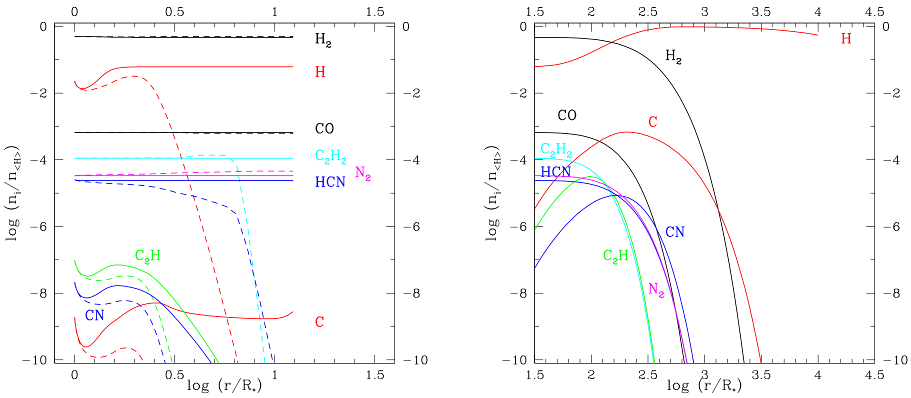

Fig. 10. Molecule concentrations in the inner region of a C-star shell (l.h.s. diagram, dashed lines are the equilibrium concentrations) and in the outer shell (r.h.s. diagram). From Patzer et al. (1996a)

first molecule to be formed. As it can be dissociated only be very energetic photons, in the absence of dissociating UV fields, CO formation acts like an "absorber" removing C and O atoms from the surroundings until either all C atoms (for oxygen–rich situations) or all O atoms (for carbon–rich situations) are consumed (cf. Fig. 11). As the CO molecule is practically chemically inert, the chemistry of the system then is determined by the residual reactive specimens which in the case of oxygen–rich systems basically yields oxides whereas in the case of carbon–rich systems predominantly carbon–hydrogen compounds, carbides and, if hydrogen is absent, other carbonaceous compounds are formed (cf. Tab 3).

Detailed network calculations show, that this key role of the CO molecule which is obvious for situations not too far from CE, generally also holds for most KE situations (Beck et al. 1992) yielding also for these systems a clear distinction of the character of the chemistry. Only for very pronounced UV fields e.g. in the late stages of a nova shell, also the CO molecule is ionized or dissociated by photo reactions, leading to a mixed oxygen–carbon chemistry in this case.

3.2 Dust nucleation and growth

3.2.1 Condensing species Astrophysical dust formation is an widespread phenomenon in particular observed in cool stellar outflows which are characteristic for red giants and supergiants. The detailed findings of corresponding

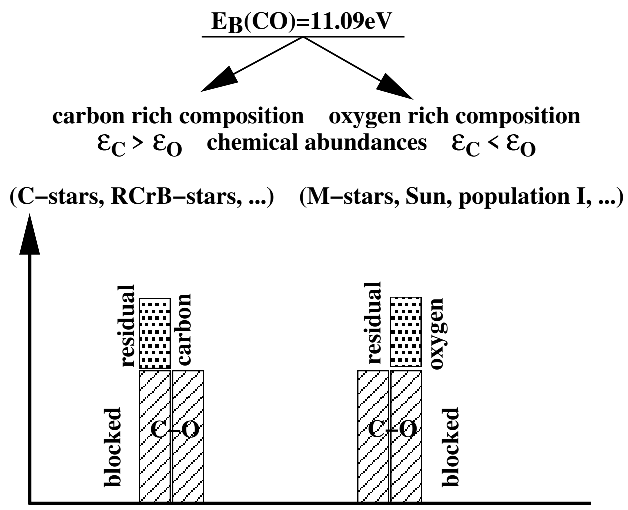

Fig. 11. Blockage by the CO molecule

Table 3. Molecules observed in the circumstellar shells of dust forming late type stars by microwave emission (e.g. Olofsson 1988)

Shells of M-stars	Shells of C-stars
H_2, CO	H_2, CO
OH, H_2O, SiO	hydrocarbons
CS, SiS, SO, SO_2, H_2S, OCS	CN, CS, SiC, SiC_2, SiS, HCO^+
HCO^+, HCN, HNC,NH_3	HCN, HNC, CH_3CN, HC_3N, HC_5N, HC_7N
	HC_9N, HC_nN, C_2H, C_3H, C_4H, C_5H, C_6H
	C_3H_2, C_3N, NH_3, C_2S, C_3S, $HSiC_2$, NaCl
	AlCl, KCl, AlF

observations demonstrate that circumstellar dust is a rather massive phenomenon being connected with substantial reddening of the stellar radiation field and hence indicating large optical depth produced by dust absorption and dust extinction. This clearly shows, that the dust component is a major constituent of the circumstellar shells, the formation of which can not be explained by rare elements alone but in any case requires the contribution of the *abundant elements*.

Circumstellar dust often is observed at temperatures around 1000 K or even higher. In order for the dust grains to survive such hostile conditions, the dust material itself must form a so–called *high temperature condensate*, i.e. it has to consist of a substance which is able to form a macroscopic particle in this temperature range.

These two criteria which are a natural outcome of the observations, have to be supplemented by an additional argument concluded from the process of grain formation, which essentially proceeds via a sequence of chemical reactions. For this being efficiently possible, the molecules involved in the various steps have not to be blocked by exceptionally high bond energies making them inert. Applying these criteria (abundant species, high temperature condensates, not too high bond energies) to the hierarchy of element abundances observed in an astronomical system yields the results for the condensing species and the primary condensates shown in Fig. 12.

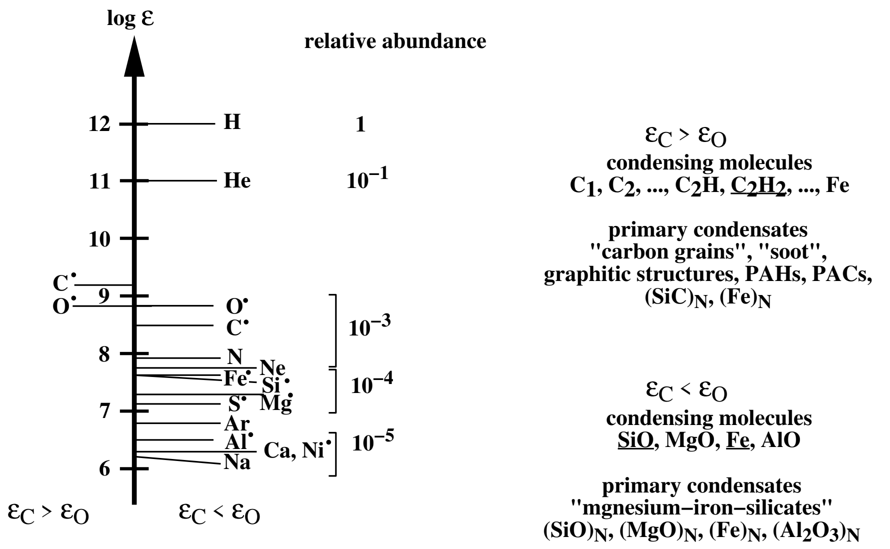

Fig. 12. Abundance hierarchy of the elements. • means, that this element is a constituent of high–temperature condensates. The leading molecules in the grain formation sequence are underlined.

3.2.2 Grain formation Basically two philosophies of description are in use for describing the formation of macroscopic grains out of the gaseous phase having both it shortcomings and its individual strengths.

The first method is a thermodynamic point of view, conceiving the solid formation as kind of a phase transition taking place if the system trajectory crosses a borderline defined by specific critical conditions for the nucleation process, usually given by a suitably defined supersaturation ratio $S = 1$. A well–known example for this are the lines separating the various aggregation states in a phase diagram e.g. for water where a gaseous, liquid and solid phase may occur, which in a natural way explains the occurrence of mist, rain, and snowflakes.

In all these situations for efficient dust formation to take place, a pronounced supersaturation ratio $S = p_{\rm i}/p_{\rm cl}$ (where $p_{\rm i}$ is the (gas) partial pressure of the condensing species i, and $p_{\rm cl}$ the corresponding vapor pressure of the considered cluster) considerably larger than unity has to be reached.

Applying this concept to circumstellar grain formation shows, that effective grain condensation usually only occurs at temperatures far below the corresponding equilibrium lines thus indicating dust condensation to be a process which efficiently proceeds generally far from thermodynamical equilibrium, a finding being in total accordance with the general behavior of structure formation in nature.

The second method is a chemical point of view, conceiving cluster formation as the result of a sequence of chemical reactions, starting in a molecular domain and resulting finally at macroscopic specimens. From this microscopic point of view grain formation could be conceived naively as a complex network of *chemical reactions* leading under favorable conditions to more and more complex aggregates which finally grow to macroscopic particles. A realization of this method is however illusory not only due to the huge number of reactions involved ($10^6 - 10^{10}$) but also due to the lack of important input data (reaction efficiency, sticking coefficients), not to mention the unrealistic computing time required for such an approach. For this reason, any successful chemical approach is restricted to the construction of some suitable chemical pathway being determined by the most efficient chain of reactions leading from molecules to macroscopic clusters. This approach requires of course

– the individual selection of the relevant molecules,
– a detailed determination of their thermodynamic functions and
– for each molecule the detailed discussion of its chemical reactions.

In order to select a certain pathway, it is essential that it contains all relevant reactions, i.e. that reactions along the pathway are much more important than reactions with other molecules. In this case the pathway is well isolated and the concentrations of the chain molecules are determined by chain processes only. For a detailed application of the chemical pathway method to the formation of polyaromatic hydrocarbons (PAHs) in C–star winds, see Fig. 14.

Irrespective of the specific treatment, the molecule–solid transition can be considered as a two step process which consists i) of the formation of small meta–stable clusters from gaseous molecules and ii) the growth of these clusters to macroscopic grains. This separation immediately follows from the thermodynamic properties of small clusters showing in the size–temperature space a critical limit line separating the regimes of dominant cluster evaporation and growth, respectively. This critical limit line defines the critical cluster by the equilibrium between evaporation and growth for given temperature. Any grain formation has to surmount the critical cluster size in order to arrive at thermodynamically stable macroscopic grains (see Fig. 13).

The regime with cluster sizes smaller than the critical cluster (i.e. where evaporation exceeds growth) is called the nucleation regime. In this regime,

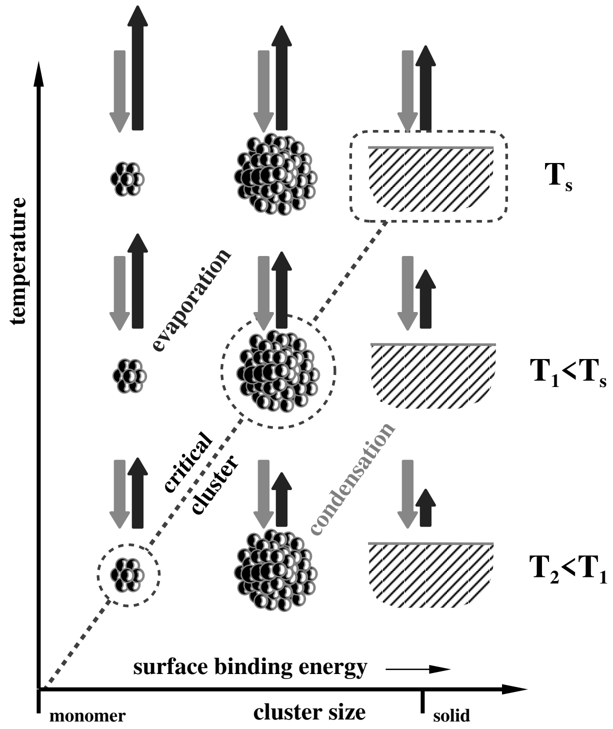

Fig. 13. Temperature dependence of the critical cluster size. T_s: sublimation temperature of the solid (adopted from Goeres 1996)

the properties of the clusters can not be described by simply applying bulk phase values but have to be determined by taking into account the individual structure of the clusters either from suitable calculations or from laboratory measurements (cf. Köhler et al. 1996, Patzer et al. 1995).

Detailed comparison of the time scales involved in the nucleation regime indicates that even in situations where moderate velocity fields are present usually the formation of the critical cluster i.e. the calculation of the nucleation rate, can be treated as a stationary problem (cf. Gail & Sedlmayr 1988, Gauger et al. 1990).

From (modified) classical nucleation theory in case of thermal and chemical equilibrium, the homogeneous nucleation rate J_* is given by

$$J_*(t) = \frac{f(1,t)}{\tau_{\mathrm{gr}}(N_*,t)} Z(N_*) \exp\left[(N_* - 1)\ln S - \frac{\Delta G(N_*)}{RT}\right] \tag{2}$$

where $f(1,t)$ is the monomer density of the condensing species (e.g. the density of C_1 in the case of soot formation), $(\tau_{\mathrm{gr}})^{-1}$ the growth time scale of the critical cluster, N_* the size of the critical cluster, Z the Zeldovich–factor (of order 1), S the supersaturation ratio and ΔG is in this notation the surface contribution to the Gibbs free energy change associated with the formation of the critical cluster from the vapor.

For homogeneous nucleation of monomers, $(\tau_{\rm gr})^{-1}$ is simply given by the product of the monomer density and the rate coefficient for the reaction between clusters of size N_* and the monomers. Gail & Sedlmayr (1988) generalized this approach to account for arbitrary chemical reactions. The influence of thermal and chemical non–equilibrium in the gas phase on the nucleation rate is discussed by Patzer et al. (1996b).

In the case of a chemical pathway approach the nucleation rate simply can be calculated by determining the rate of the slowest step on the most efficient pathway

$$J_* = \frac{f(N_*)}{\tau} \tag{3}$$

where $f(N_*)$ is the particle density of the critical cluster and τ is the characteristic formation time of clusters of size N_* from clusters of size N_*-1.

Like in classical nucleation theory also in the pathway description the critical cluster determines a "bottleneck" separating the nucleation regime and the growth regime. This bottleneck has to be surmounted for effective grain growth to occur.

As an example of a chemical pathway, in Fig.14 the formation of polyaromatic hydrocarbons (PAHs) is shown (Goeres 1993).

3.2.3 Grain growth Well beyond the critical cluster in all cases under consideration grain growth can reliably be treated by a thermodynamic approach. In this context the number densities of grains of size N are conceived as "level populations" which are changed by gain and loss processes:

$$\frac{d\,f(x,N,t)}{dt} = R_\uparrow - R_\downarrow + R^\downarrow - R^\uparrow \quad . \tag{4}$$

Figure 15 gives a schematic representation of the level diagram indicating gain and loss processes by transitions caused by the addition and the evaporation of molecules, respectively. Due to these processes, the actual local occupation density $f(x,N,t)$ of level N obeys an equation of continuity

$$\frac{d\,f(x,N,t)}{dt} = \frac{\partial f(x,N,t)}{\partial t} + \mathrm{div}\,(v\,f(x,N,t)) = \sum_{i=1}^{I} J_{N,i}(x,t) - \sum_{i=1}^{I} J_{N+i,i}(x,t) \tag{5}$$

with $\sum_{i=1}^{I} J_{N,i}$ being the net gain rate of level N from the levels below and I is the maximum i-mer changing the cluster size. The time derivative $d(\cdot)/dt = \partial(\cdot)/\partial t + \mathrm{div}\,(v\,\cdot)$ on the l.h.s. comprises both, the explicit change with time and the net gain due to surface fluxes via the mass flow of velocity v.

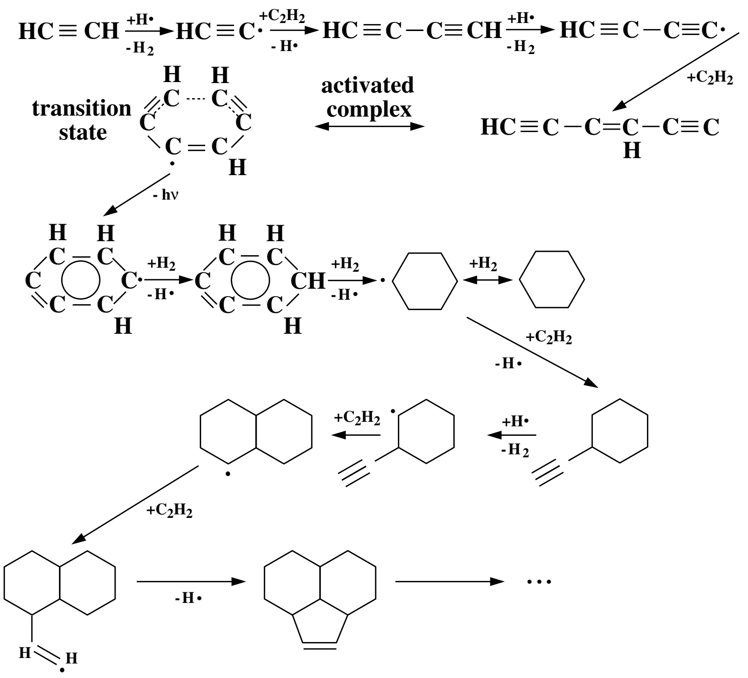

Fig. 14. Chemical pathway to PAH formation (adopted from Goeres 1993)

The rates $J_{N,i}$ are given by

$$J_{N,i}(x,t) = f(i)\, v_{N-i,i} A_{N-i} \alpha_{N-i,i} \left(f(N-i) - \frac{\overset{\circ}{f}\,(N-i)}{\overset{\circ}{f}\,(N)} f(N) \right) \qquad (6)$$

where $f(i)$ is the density of the growth species, $v_{N-i,i}$ is the relative velocity between growth species i and a cluster of size $N-1$, A_{N-i} is the surface of a cluster with size $N-i$, $\alpha_{N-i,i}$ is the respective sticking efficiency, and $\overset{\circ}{f}\,(\cdot)$ denotes the respective distribution function in thermal equilibrium. In Eq. 6 LTE is assumed. More general expressions are discussed in Gail & Sedlmayr (1988), Gauger et al. (1990), and Patzer et al. (1996b).

In most astrophysical applications it is not necessary to solve the full network of rate equations Eq. (5) but it is sufficient to define suitable moments by summation over the cluster size space according to

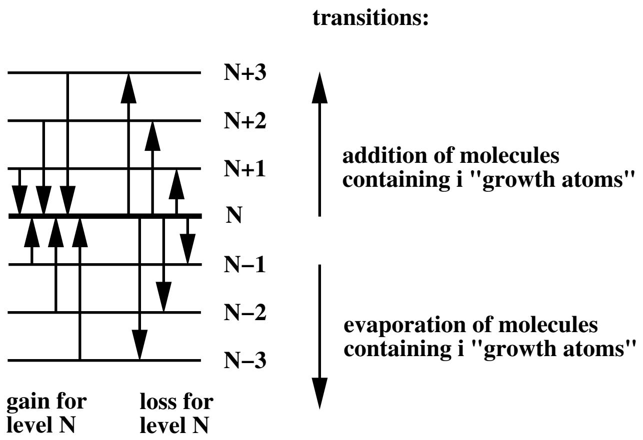

Fig. 15. Level representation of the cluster size space, possible transitions between the levels, and effective rates with respect to level N.

$$K_j(x,t) = \sum_{N=N_\ell}^{N_{max}} N^{j/d} f(x,N,t) \qquad (j = 0,1,2,\ldots) \tag{7}$$

with d being the dimension of the considered clusters ($d = 3$ for 3–dimensional particles, $d = 2$ for 2-dimensional, e.g. flat particles) and N_ℓ is a lower limit size for the dust grains to be considered as macroscopic particles (usually $N_\ell \approx 1000$). Introducing these moments into Eq. (5) yields the system of moment equations describing grain growth in arbitrary moving media

$$\frac{dK_j}{dt} = \frac{j}{d\,\tau_{\rm gr}} K_{j-1} + N_\ell^{j/d} J_{N_\ell} \quad , \tag{8}$$

where the time scale for particle growth is given by

$$\frac{1}{\tau_{\rm gr}} = \sum_{i=1}^{I} A_1 v_i \alpha_i i f(i) \quad . \tag{9}$$

A good approximation for this system, applicable to most astrophysical situations is given by

$$\frac{dK_j}{dt} = \begin{cases} J_* \ , & j = 0, \\ \frac{j}{\tau_{\rm gr}\, d} K_{j-1} \ , & j > 0 \end{cases} \tag{10}$$

The first four moments have simple physical interpretations:

$$
\begin{aligned}
&K_0 = n_{\rm d} = \text{dust number density}\\
&\frac{K_1}{K_0} = < N^{1/d} > \propto < \text{size} >\\
&\frac{K_2}{K_0} = < N^{2/d} > \propto < \text{surface} >\\
&\frac{K_3}{K_0} = < N^{3/d} > \stackrel{\text{d=3}}{\propto} < \text{volume} > \propto \text{extinction coefficient}
\end{aligned}
$$

3.2.4 Cluster size spectrum In the case, that grain evaporation can be neglected, (e.g. in a stationary wind) the moment equation for $j = 0$

$$\frac{dK_0}{dt} = J_* \tag{11}$$

allows a straight–forward calculation of the grain size spectrum $f(N)$ (a complete treatment including the effects of grain evaporation is given in Gauger et al.(1990)):

The growth of an individual grain of size N simply is given by:

$$\frac{dN}{dt} = \frac{1}{\tau_{\rm gr}} N^{\frac{d-1}{d}} \tag{12}$$

from which we get

$$\frac{d(N^{1/d})}{dt} = \frac{1}{d\,\tau_{\rm gr}} \tag{13}$$

Defining the grain radius by $a = a_0 N^{1/d}$, where a_0 is the hypothetical radius of a monomer, we obtain for the time evolution of the particle size

$$\frac{da}{dt} = \frac{1}{\tau_{\rm gr}} \frac{a_0}{d} \tag{14}$$

Now assume that a cluster is created at time t_0 with size N_*. With this initial condition, Eq.(13) immediately can be integrated:

$$N(t,t_0) = \left\{ \frac{1}{d} \int_{t_0}^{t} dt' \frac{1}{\tau_{\rm gr}(t')} + N_*^{1/d} \right\}^d \quad . \tag{15}$$

$N(t,t_0)$ denotes the size of the particle at time t, which has formed with size N_* at time t_0. Due to our assumption of monotonic growth, all particles smaller than $N(t,t_0)$ at time t must have been created later than t_0. Thus, for the number of particles with sizes between N_* and $N(t,t_0)$ we obtain

$$\Delta K_0(N_*, N(t,t_0)) = \int_{t_0}^{t} dK_0 = \int_{N_*}^{N(t,t_0)} f(N,t)dN = \int_{t_0}^{t} J_*(t')dt' \quad . \tag{16}$$

Differentiating Eq. (16) with respect to t_0 yields

$$J_*(t_0) = -\frac{d(N(t,t_0))}{dt_0} f(N(t,t_0),t) \quad . \tag{17}$$

Solving this for the distribution function $f(t,N)$ yields

$$f(N(t,t_0),t) = \left(-\frac{d(N(t,t_0))}{dt_0}\right)^{-1} J_*(t_0) = \tau_{\rm gr}(t_0) N(t,t_0)^{\frac{1-d}{d}} J_*(t_0) \quad , \tag{18}$$

where the second equality follows from Eq. (15).

Thus, in an actual model calculation, one just has to integrate Eq. 12 along the flow trajectory (i.e. in each fixed volume element) and to store the current values of J_* and $\tau_{\rm gr}$ in order to obtain the current size distribution in each gas element. As an example, Fig. 16 depicts the size distribution function resulting from a model calculation for a stationary dust–driven wind (see Sect. 4.3).

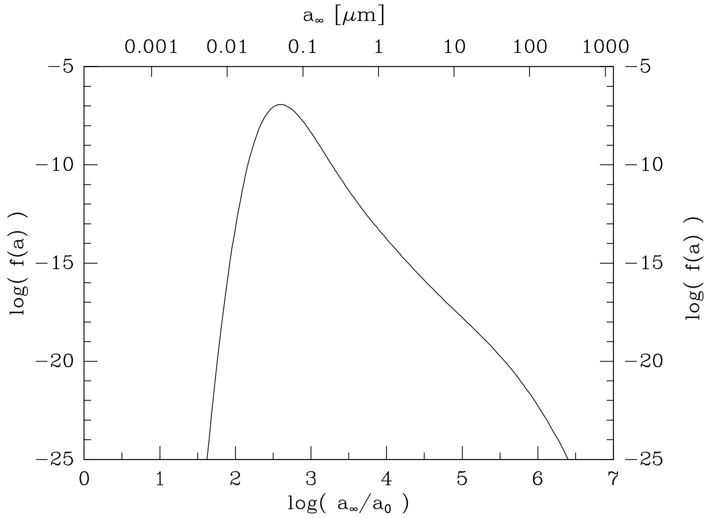

Fig. 16. Grain size distribution function in the outer region of a stationary dust driven wind model. a_∞ is the final particle size reached in an outer volume element, where grain nucleation and growth have ceased.

For this calculation, the grains are assumed to consist of amorphous carbon and classical nucleation theory (cf. Sect. 3.2.2) has been applied to calculate the grain formation rate. The resulting size distribution function can well be approximated by a power law $f(a) \propto a^{-5}$ in the size range $0.05\mu\text{m} < a < 100\mu\text{m}$, a typical result for a stationary dust driven wind (see Dominik et al. 1989). Although most particles have radii of about 0.05μm, there exists a considerable number of particles having much larger radii. These large particles are formed in the innermost region of the circumstellar dust shell (inside the sonic point), where the outflow velocity is still small and, therefore, the particles remain for a rather long time in a region of favorable growth conditions (for a detailed discussion see Dominik et al. (1989) and Winters et al. (1994a)).

4 Modeling of dust shells around late type giants

In this section we present the self-consistent description of cool, extended dust forming circumstellar shells, including a detailed treatment of

- hydrodynamics
- thermodynamics
- radiative transfer
- chemistry
- dust nucleation and growth.

The complete problem to be treated is sketched in Fig. 6. In the following we give the mathematical formulation of this problem and present typical numerical results for stationary dust driven winds and pulsating atmospheres around long–period variable stars. In both cases, spherical symmetry of the central star and its surrounding shell is assumed.

4.1 Basic equations

4.1.1 Hydrodynamic equations From the law of mass conservation, the equation of continuity is given, which in spherical symmetry reads

$$\frac{\partial \rho}{\partial t} + \frac{1}{r^2}\frac{\partial}{\partial r}(r^2 \rho v) = 0 \ . \tag{19}$$

Here, t is the time, r is the radial coordinate, $\rho(r,t)$ is the mass density and $v(r,t)$ is the outflow velocity. In a **stationary situation** (i.e. $\partial/\partial t = 0$), Eq. (19) can be integrated to yield

$$\int_0^r dr' 4\pi r'^2 \left(\frac{1}{r'^2}\frac{\partial}{\partial r'}(r'^2 \rho v) \right) = 4\pi r^2 \rho v = \mathrm{const} = \dot{M} \ , \tag{20}$$

where $\dot{M}$ is the integration constant, describing the total mass transport through the surface of radius r. Thus, $\dot{M}$ is the mass loss rate of the star. In general, the value of the mass loss rate depends on the fundamental stellar parameters: stellar mass M_*, stellar luminosity L_*, stellar temperature T_*, and the element abundances $\{\epsilon_i\}$.

Momentum conservation provides us with the equation of motion:

$$\frac{\partial v}{\partial t} + v\,\frac{\partial v}{\partial r} = -\frac{1}{\rho}\frac{\partial p}{\partial r} + a \tag{21}$$

with $p(r,t)$: thermal pressure and $a(r,t)$: acceleration due to *external* forces.

For the conditions typical of a circumstellar shell, the equation of state, relating thermal pressure, mass density, and gas temperature, is given by the ideal gas law

$$p = \frac{\rho}{\bar{\mu} m_{\rm H}} kT \tag{22}$$

with $\bar{\mu}(r,t)$: mean molecular weight, $T(r,t)$: gas kinetic temperature, and $m_{\rm H}$: mass of a hydrogen atom.

The acceleration $a(r,t)$ usually consists of the contribution of two different external forces

$$a = -g + a_{\rm rad} \tag{23}$$

with the local (inwards directed) gravitational acceleration

$$g = G\frac{M_* + M_{\rm s}(r,t)}{r^2} \tag{24}$$

caused by the stellar mass M_* and the mass contained in the circumstellar shell inside the radial surface at r

$$M_{\rm s}(r,t) = \int_{R_*}^{r} dr' 4\pi r'^2 \rho(r',t) \tag{25}$$

and the (outward directed) radiative acceleration $a_{\rm rad}(r,t)$ of the matter due to photon momentum extinction. In practice, Eq. (23) is usually written as

$$a = -g(1-\alpha) \tag{26}$$

with

$$\alpha(r,t) = \frac{a_{\rm rad}}{g} = \frac{4\pi}{cGM_*}\frac{\chi_H}{\rho} r^2 H \tag{27}$$

being the radiative acceleration measured in units of the local gravitational acceleration. The quantity H is the frequency integrated Eddington flux

$$H = \int_0^\infty d\nu H_\nu \tag{28}$$

and χ_H the flux–mean extinction coefficient

$$\chi_H = \frac{1}{H}\int_0^\infty d\nu \chi_\nu H_\nu \quad . \tag{29}$$

The extinction coefficient

$$\chi_\nu = \kappa_\nu + s_\nu \tag{30}$$

is the sum of the absorption coefficient κ_ν and the scattering coefficient s_ν. Both, κ_ν and s_ν consist of all respective contributions from the gaseous species and the various dust components.

The absorption and scattering cross sections of a dust grain is huge compared to those of an atom or molecule. Therefore, if a noticeable amount of dust is present in a stellar atmosphere, it completely dominates the transport coefficients.

The transport coefficients of the dust components depend on the local size distribution of the grains:

$$\chi_\nu^{\mathrm{d}} = \int_{a_\ell}^\infty da f(a)\sigma_{\mathrm{ext}}^{\mathrm{d}}(\nu, a) \tag{31}$$

$$s_\nu^{\mathrm{d}} = \int_{a_\ell}^\infty da f(a)\sigma_{\mathrm{sca}}^{\mathrm{d}}(\nu, a) \tag{32}$$

$$\kappa_\nu^{\mathrm{d}} = \chi_\nu^{\mathrm{d}} - s_\nu^{\mathrm{d}} = \int_{a_\ell}^\infty da f(a)\sigma_{\mathrm{abs}}^{\mathrm{d}}(\nu, a) \quad . \tag{33}$$

The cross sections $\sigma_{\dots}^{\mathrm{d}}$ usually are expressed as the product of the geometric cross section πa^2 of the particle (assumed here to be spherical with radius a) and an efficiency Q describing the interaction with the radiation field. These efficiency factors follow from Mie theory (see e.g. Bohren & Huffman (1983)) and the size distribution function $f(a)$ is calculated according to the method given in Sect. 3.2.4.

For grains small compared to the wavelength of the radiation field (i.e. $a \ll \lambda/2\pi$) the *small particle limit* of Mie theory applies and the transport coefficients can be written as

$$\chi_\nu^{\mathrm{d}} = A(\nu)\int da\, a^3 f(a) = A(\nu)\hat{K}_3 \tag{34}$$

$$s_\nu^{\mathrm{d}} = B(\nu)\int da\, a^6 f(a) = B(\nu)\hat{K}_6 \tag{35}$$

while in the opposite case of the *large particle limit* of Mie theory (i.e. $a \gg \lambda/2\pi$)

$$\kappa_\nu^{\mathrm{d}} = s_\nu^{\mathrm{d}} = \int da\, \pi a^2 f(a) = \pi\hat{K}_2 = \frac{1}{2}\chi_\nu^{\mathrm{d}} \tag{36}$$

holds. The "radius" moments

$$\hat{K}_j = \int da\, a^j f(a) \tag{37}$$

are related to the moments K_j defined in Sect. 3.2.3 via

$$\hat{K}_j = a_0^j K_j \qquad \text{j=0, 1, 2, \ldots} \tag{38}$$

where a_0 is the hypothetical radius of a monomer contained in a grain.

In a stationary situation, it is convenient to transform the equation of motion Eq. (21) into the so–called *wind equation*. This is accomplished by introducing the isothermal sound speed

$$c_T^2 = \frac{p}{\rho} \tag{39}$$

and making use of the equation of continuity Eq. (19) (where of course $\partial\rho/\partial t = 0!$). The result is

$$(v^2 - c_T^2)\frac{1}{v}\frac{\partial v}{\partial r} = \frac{2}{r}c_T^2 - \frac{\partial c_T^2}{\partial r} - g(1-\alpha) \tag{40}$$

with the *critical point* r_c defined by the (implicit) conditions

$$v(r_c) = c_T(r_c) \tag{41}$$

and

$$\frac{2}{r_c}c_T^2(r_c) - \left.\frac{\partial c_T^2}{\partial r}\right|_{r_c} - g(r_c)(1-\alpha(r_c)) = \phi(r_c) = 0 \tag{42}$$

(see also the lecture of H. Lamers). If we neglect the temperature variation in Eq. (42), r_c is determined by the implicit equation

$$\alpha(r_c) = 1 - 4\frac{r_c}{R_*}\left(\frac{c_T(r_c)}{v_e(R_*)}\right)^2 \tag{43}$$

with the escape velocity at the stellar surface

$$v_e = [2R_* g(R_*)]^{1/2} \ . \tag{44}$$

Self-consistent model calculations indicate, that for a dust driven wind the second term in Eq. (43) is always small compared to unity (thermally stable atmosphere!), i.e.

$$\alpha(r_c) \approx 1 \tag{45}$$

is a necessary condition for a dust driven wind to exist.

4.1.2 Thermodynamic equations The law of energy conservation provides us with an equation for the temperature of the gas and the dust. The balance equation for the *thermal* energy is given by

$$\frac{\partial(\rho e)}{\partial t} + \frac{1}{r^2}\frac{\partial}{\partial r}(r^2\rho v h) - v\frac{\partial p}{\partial r} = Q_e \ , \tag{46}$$

where e is the specific energy and $h = e + p/\rho$ the specific enthalpy with $h = c_p T$ for an ideal gas. c_p is the specific heat for constant pressure and Q_e the local net energy input rate per unit volume due to external energy sources.

In the stationary case, Eq. (46) can be written as

$$v\left(\rho c_p \frac{\partial T}{\partial r} - \frac{\partial p}{\partial r}\right) = Q_e \tag{47}$$

where Eq. (20) has been used.

In a stationary dust driven wind radiative equilibrium holds (i.e. $Q_e = 0$), and the source term in Eq. (47) can be written as

$$Q_e = \varGamma_e - \varLambda_e = 0 = \int_0^\infty d\nu\,(\kappa_\nu^{\rm g} + \kappa_\nu^{\rm d})J_\nu - \int_0^\infty d\nu\,(\epsilon_\nu^{\rm g} + \epsilon_\nu^{\rm d}) \tag{48}$$

where the gain and loss rates ($\varGamma_e$ and $\varLambda_e$) are given by the absorption and emission of radiation energy. In writing Eq. (48), elastic scattering of the photons is assumed. J_ν is the monochromatic mean intensity of the radiation field (cf. Eq. (51)) and ϵ_ν is the emission coefficient (g and d refer to the gas and the dust component, respectively). In many cases the dust component decouples thermally from the gas and the energy balance for the dust alone is given by

$$\int_0^\infty d\nu\,\kappa_\nu^{\rm d} J_\nu = \int_0^\infty d\nu\,\epsilon_\nu^{\rm d} = \int_0^\infty d\nu\,\kappa_\nu^{\rm d} B_\nu(T^{\rm d}) \tag{49}$$

where $B_\nu(T^{\rm d})$ is the Kirchhoff–Planck function at the internal dust temperature $T^{\rm d}$. Eqs. (48) and (49) are an implicit system for the "gas temperature" $T(r)$ and the "dust temperature" $T^{\rm d}(r)$.

4.1.3 Radiative transfer For the situations considered here, it is sufficient to consider the stationary radiative transfer equation (i.e. $\partial I_\nu/\partial t = 0$), since the transport coefficients vary on a time scale which is longer than the time needed for the photons to travel through the region where these changes occur. In the case of isotropic absorption, scattering and emission, the stationary radiative transfer equation in spherical symmetry is given by

$$\mu\frac{\partial I_\nu(r,\mu)}{\partial r} + \frac{1-\mu^2}{r}\frac{\partial I_\nu(r,\mu)}{\partial \mu} = -(\kappa_\nu + s_\nu)I_\nu(r,\mu) + \epsilon_\nu + s_\nu J_\nu(r) \tag{50}$$

with the angle variable $\mu = \cos\theta$, where θ is the angle between the radial vector and the direction of light propagation, and the monochromatic mean intensity defined by

$$J_\nu(r) = \frac{1}{2}\int_{-1}^{+1} d\mu\, I_\nu(r,\mu) \tag{51}$$

For given transport coefficients, the partial integro–differential equation (50) has to be solved numerically for the specific monochromatic intensity $I_\nu(r,\mu)$. This can be accomplished e.g. by the Feautrier method, which involves an iteration between the solution of Eq. (50) along the characteristic paths and the equations for the moments of $I_\nu(r,\mu)$ defined by

$$M_\nu^n(r) = \frac{1}{2}\int_{-1}^{+1} d\mu\, \mu^n I_\nu(r,\mu) \tag{52}$$

(for details see the standard textbook by Mihalas (1978)).

4.1.4 Chemistry In general, the number densities of the molecules are given by the solution of the chemical rate network Eq. (1) (see Sect. 3.1). In the special situation of chemical equilibrium, the rate network is replaced by the law of mass action which, if completed by the conservation of the elements reads

$$n_{<\mathrm{i}>} - \sum_{j=1}^{N} \nu_i \nu_j n_i n_j K_{\mathrm{eq}}(i,j) = 0 \ , \tag{53}$$

where ν_k are the stoichiometry coefficients and K_{eq} is the equilibrium constant.

4.1.5 Dust formation and growth As discussed in Sect. 3.2, formation and growth of dust grains is described by the set of moment equations

$$\begin{aligned} \frac{dK_0}{dt} &= J_* \\ \frac{dK_j}{dt} &= \frac{j}{d\tau_{\mathrm{gr}}} K_{j-1} \end{aligned} \tag{54}$$

which by consumption of the dust forming elements is coupled to the chemistry. In the simple case of homomolecular, homogeneous condensation of carbon, the consumption equation is given by

$$\frac{dn_{<\mathrm{C}>}}{dt} = -\frac{dK_3}{dt} \ . \tag{55}$$

The chemistry and dust complex are solved considering a fixed mass element, i.e. in a co-moving frame (remember: $d\cdot/dt = \partial\cdot/\partial t + div(\cdot v)$)

The fundamental equations given in this section form the complete set necessary for the modeling of dust forming circumstellar shells. Of course, this set has to be solved by applying suitable boundary conditions, and in the case of a time–dependent description, also suitable initial conditions.

4.2 External parameters

The self-consistent solution of this set of equations (i.e. the shell model) is completely determined by the prescription of 4 fundamental stellar parameters, e.g. the sets given in Tab. 4.

Table 4. Examples for different combinations of parameters describing a dust driven wind

M_*	or	M_*	or	M_*	or	$\dot{M}$	etc.
T_*		$\dot{M}$		R_*		T_*	
L_*		L_*		L_*		L_*	
$\{\ldots,\epsilon_i\ldots\}$		$\{\ldots,\epsilon_i\ldots\}$		$\{\ldots,\epsilon_i\ldots\}$		$\{\ldots,\epsilon_i\ldots\}$	

Depending on the specific problem a suitable set of basic parameters is chosen. Besides these 4 prescribed parameters all other quantities are determined by the solution of the set of fundamental equations. Results of this approach applied to stationary dust driven winds are given in Sect. 4.3. For the time–dependent modeling of circumstellar dust shells around pulsating long–period variable stars, assumed to exhibit a sinusoidal temporal variation inside the photosphere, two additional parameters have to be prescribed in order to simulate the pulsation of the star. This is necessary, since the current models only describe the circumstellar dust shell (CDS) but not the region well inside the photosphere, where the pulsation of the star is generated. Results of these time–dependent model calculations are presented in Sect. 4.4

4.3 Stationary dust–driven winds

4.3.1 The minimum mass loss rate In a dust driven wind, the only driving mechanism of the outflow is radiation pressure on the dust grains which is transferred to the ambient gas by momentum coupling between dust and gas. Other effects, like momentum and energy input to the atmosphere by wave dissipation are neglected. Therefore, we can derive a minimum luminosity or, equivalently, a minimum mass loss rate which has to be surmounted in order for a dust driven wind to exist (cf. Gail & Sedlmayr 1987, Dominik et al. 1990). From the definition of the radiative acceleration (Eq. (27)) we get

$$\begin{aligned}\alpha &= \frac{4\pi}{cGM_*}\frac{\chi_H}{\rho}r^2 H \\ &= \frac{4\pi}{cGM_*}\frac{\chi_H}{\rho}R_*^2 H_* \\ &= \frac{\chi_H}{4\pi cG\rho M_*}L_*\end{aligned} \tag{56}$$

where the condition of radiative equilibrium

$$r^2 H(r) = \text{const} = R_*^2 H_* \tag{57}$$

and the definition of the stellar luminosity

$$L_* = 16\pi^2 R_*^2 H_* \tag{58}$$

have been used. If dust is present, the extinction coefficient χ_H is essentially given by the dust component (i.e $\chi_H \approx \chi_H^{\mathrm{d}}$) which is proportional to the local amount of dust, i.e. the degree of condensation f_{c}:

$$f_{\mathrm{c}} = \frac{K_3}{K_3^{\max}} = \frac{\chi_H}{\chi_H^{\max}} \quad . \tag{59}$$

Inserting Eq. (59) into Eq. (56) yields

$$\alpha = f_{\mathrm{c}} \frac{\chi_H^{\max}}{4\pi c G \rho M_*} L_* \tag{60}$$

$$= f_{\mathrm{c}} \frac{L_*}{L_{\mathrm{edd}}} \tag{61}$$

where we have defined the so–called Eddington luminosity

$$L_{\mathrm{edd}} = \frac{4\pi c G \rho M_*}{\chi_H^{\max}} \tag{62}$$

which is the maximum luminosity for an atmosphere stable against radiation induced expansion (cf. Eq. (26): $\alpha = 1 \leftrightarrow a = 0$!).

According to Eq. (45) a dust driven wind requires

$$\alpha(r_c) = f_{\mathrm{c}}(r_c) \frac{L_*}{L_{\mathrm{edd}}} \geq 1 \quad . \tag{63}$$

Thus, for a given value of f_{c} we get the desired minimum luminosity required to drive the wind solely by radiation pressure:

$$L_*^{\min} = \frac{L_{\mathrm{edd}}}{f_{\mathrm{c}}(r_c)} \quad . \tag{64}$$

The r.h.s. of Eq. (64) is essentially determined by M_* and $\dot{M}$. Since $\dot{M}$ is a function of the stellar parameters ($\dot{M} = f(L_*, T_*, M_*, \{\ldots, \epsilon_{\mathrm{i}}, \ldots\})$), for given stellar mass M_* and element abundances $\{\ldots, \epsilon_{\mathrm{i}}, \ldots\}$ a contour line

$$\dot{M}^{\min} = f(L_*^{\min}, T_*) \tag{65}$$

of minimum mass loss rate exists in the HRD, which confines objects producing dust driven winds to the region above this limiting line, i.e. to the region of high luminosities. This minimum mass loss rate typically is of the order of $10^{-7} \ldots 10^{-6} M_\odot \mathrm{yr}^{-1}$.

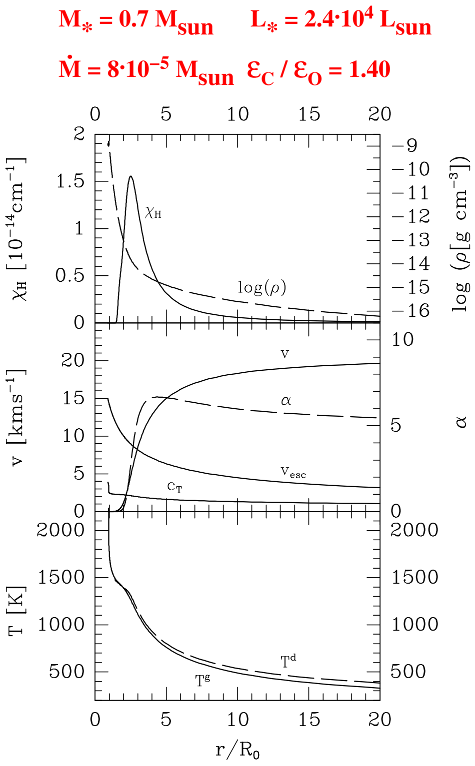

Fig. 17. Radial structure of a stationary dust driven wind model for IRC +10216. **Upper diagram:** flux-mean extinction coefficient χ_H of the dust component (solid line, l.h.s. ordinate) and logarithm of the density ρ (dashed line, r.h.s. ordinate); **middle diagram:** hydrodynamic velocity v and velocity of sound c_T (solid line, l.h.s. ordinate) and radiative acceleration in units of the local gravitational deceleration α (dashed line, r.h.s. ordinate); **lower diagram:** temperature of the gas (solid line) and the dust component (dashed line). (adopted from Winters et al. 1994).

4.3.2 Typical shell structure of a dust driven wind Figure 17 shows the radial structure of a dust driven wind model designed to describe the observational data of the prototype of extreme carbon stars IRC +10216 (Winters et al. 1994a).

The formation of dust grains starts around $1.4R_0$ ($R_0 = 9.25 \cdot 10^{13}$cm), which leads to a steep increase of the dust extinction $\chi_{\rm H}$ and, therefore, of the radiative force accelerating the dust grains. By momentum coupling of the grains to the surrounding gas, the momentum gained by the dust particles is transferred to the gas. This process results in an outward directed net acceleration ($\alpha > 1$ for $r > 2.25R_0$) of the grain-gas mixture leading to an increasing outflow velocity v of the material. The transition from sub-sonic to supersonic motion occurs at $r = r_c = 2.2R_0$ where α reaches a value of 0.75. Around $3R_0$ the wind velocity exceeds the local escape velocity v_{esc}. The atmospheric material, therefore, is lifted out of the stellar gravitational field within the first two stellar radii above the photosphere. The final outflow velocity of $20.7\,\mathrm{kms}^{-1}$ is nearly reached at $20R_0$.

The essential acceleration of the material occurs in the region between $2R_0$ and $5\,R_0$. In the region of effective dust formation and growth (around $r = 2.5R_0$) the gas temperature is $T^{g} \approx 1300\mathrm{K}$, while the mass density in this region is about $10^{-14}\mathrm{gcm}^{-3}$. Thermal dust emission from the inner edge of the circumstellar shell heats the gas inside the dust formation zone. The dust opacity, thus, leads to a substantial backwarming which results in an almost constant temperature throughout the region of effective dust formation. The size–independent dust temperature T^{d} (cf. Eq. (49)) exceeds the (grey) gas temperature. The temperature difference produced by this greenhouse effect increases with increasing distance from the photosphere. The temperature difference between gas and dust reaches a maximum value of about 50K in this model.

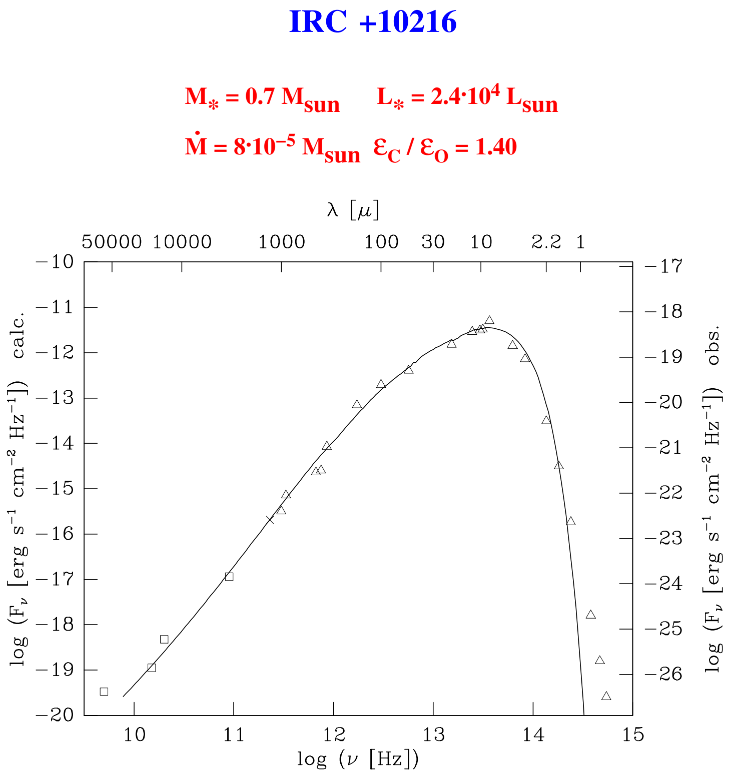

Fig. 18. Emergent spectrum of the dust shell model described in the text (solid line). The observed data for IRC +10216 are taken from Le Bertre 1987 and references therein ($\triangle$), Sahai et al. 1989 ($\square$) and Walmsley et al. 1991 ($\times$).

In Fig. 18 the spectral energy distribution produced by the dust shell model is shown together with observed photometric data of IRC +10216. This source is known to be variable with a period of $\sim$ 640d (Witteborn et al. 1980; Ridgway & Keady 1988). The symbols shown in Figs. 18 represent fluxes measured near the maximum of the 2.2μm light curve. The calculated spectrum results from assuming amorphous carbon described by the complex refractive index tabulated in Maron (1990). The outer boundary of the dust shell model is located at $2 \cdot 10^3 R_0$ which corresponds to a distance from the center of the star of $1.85 \cdot 10^{17}$cm. The synthetic spectrum of this model is in close agreement with the observed spectrum of IRC +10216 in the wavelength region between 2μm and 5cm. In the near infrared region short-ward of $\lambda \approx$ 2μm the calculated spectrum decreases much too steeply as compared to the observed fluxes. This behavior may be due to the existence of rather large dust particles in the inner part of the dust shell model, which is a result of the assumption of stationarity. A second, probably more important reason could be our assumption of spherical geometry, which cannot account for possible 'holes' in the dust shell, which would produce smaller optical depths along certain lines of sight in direction to the central object. In consequence, short wavelength radiation originating from the photosphere could escape through such holes and thus could lead to an emergent short wavelength flux which is possibly considerably enhanced compared to the flux resulting from a spherically symmetric model. From the absolute values of the calculated and observed fluxes we derive a distance to IRC +10216 of $d = 170$pc.

4.3.3 Dependence of the models on the stellar parameters Generally, the stationary dust driven wind represents the solution of a fully coupled non–linear problem which results in a rather intricate dependence of the models on the individual stellar parameters. In the following, we describe the qualitative dependence of important shell characteristics on the parameters chosen (M_*, L_*, $\dot{M}$, $\epsilon_{\rm C}/\epsilon_{\rm O}$, the other elements (including oxygen) are assumed to have solar abundances). In the following, $\uparrow$ means increasing, $\downarrow$ means decreasing. (An explicit description of these dependences is given in Winters et al. (1994a).)

stellar mass M_*: For realistic values, M_* has only a minor influence on the model structure and the shell spectrum. However, for each given luminosity L_*, there exists a maximum mass $M_{*,\rm max}$ above which no dust driven wind exists.
$M_* \uparrow \rightarrow v_\infty \downarrow \rightarrow$ grain growth$\uparrow \rightarrow f_{\rm c} \uparrow \rightarrow \chi_H^{\rm max} \uparrow \rightarrow$(absorption$\uparrow$ and $T_* \downarrow$) $\rightarrow$ "cooling" of the spectrum
$M_* \uparrow \rightarrow (\alpha \propto 1/M_*) \downarrow$ (almost linear, cf. Eq. (27))

stellar luminosity L_*:
$L_* \uparrow \rightarrow \alpha \uparrow$ (cf. Eq. (56)) $\rightarrow v \uparrow$ (inside the sonic point) $\rightarrow$ dilution $\uparrow \rightarrow$ collision rate $\downarrow \rightarrow$ effective growth $\downarrow \rightarrow$ (grain size, $f_{\rm c}$) $\downarrow \rightarrow \chi_H \downarrow \rightarrow \alpha_\infty \propto L_*(\chi_H/\rho)$ nearly

unchanged and v_∞ nearly unchanged
$L_* \uparrow \rightarrow \ldots \rightarrow \chi_H \downarrow (\kappa_H \downarrow) \rightarrow \tau \downarrow \rightarrow$ shell more transparent
$L_* \uparrow \rightarrow T_* \uparrow$, together with the above $\rightarrow$ "hotter" spectrum

mass loss rate $\dot{M}$:
$\dot{M} \uparrow \rightarrow \rho \uparrow \rightarrow$ collision rate$\uparrow \rightarrow$ growth$\uparrow \rightarrow$ grain size$\uparrow \rightarrow f_c \uparrow \rightarrow \chi_H, \kappa_H \uparrow \rightarrow \alpha(r >$sonic point$) \uparrow \rightarrow v_\infty \uparrow$
$\dot{M} \uparrow \rightarrow \ldots \rightarrow \chi_H, \kappa_H \uparrow \rightarrow$ shell spectrum becomes "cooler"

carbon abundance ϵ_C:
$\epsilon_\mathrm{C} \uparrow \rightarrow (\epsilon_\mathrm{C} - \epsilon_\mathrm{O}) \uparrow \rightarrow (n_\mathrm{C} = K_3^\mathrm{max} = (\epsilon_\mathrm{C} - \epsilon_\mathrm{O}) n_{<\mathrm{H}>}) \uparrow$ and $J_*^\mathrm{max} \uparrow \rightarrow f_c \uparrow \rightarrow \chi_H \uparrow \rightarrow \alpha \uparrow \rightarrow v \uparrow^1 \rightarrow$ dilution$\uparrow \rightarrow$ collision rate in co–moving element$\downarrow \rightarrow$ growth$\downarrow \rightarrow$ grain size$\downarrow$
[1]result: $v_\infty = A(T_*, L_*) \frac{\epsilon_\mathrm{C} - \epsilon_\mathrm{O}}{\epsilon_\mathrm{O}}$
hence: $\epsilon_\mathrm{C} \uparrow \rightarrow \kappa^\mathrm{d}_{\lambda\mathrm{short}} \uparrow \rightarrow$ (NIR and visible light)$\downarrow$ and simultaneously $\epsilon^\mathrm{d}_{\lambda\mathrm{long}} \uparrow \rightarrow$ (FIR emission)$\uparrow$.

In the preceding section, we have chosen the quadruple $M_*, L_*, \dot{M}, \{\ldots \epsilon_\mathrm{i}, \ldots\}$ as the set of parameters. Choosing the set $M_*, L_*, T_*, \{\ldots \epsilon_\mathrm{i}, \ldots\}$ allows a direct investigation of the dependence of the mass loss rate on the classical stellar parameters. The result is, that the mass loss rate of a dust driven wind increases with increasing stellar luminosity, decreasing stellar temperature and decreasing stellar mass. Since the AGB evolution leads to increasing luminosities and (slightly) decreasing temperature, the mass loss rate strongly increases along the AGB evolution of a star. The mass loss process is self–accelerating: due to mass loss, the mass of the star decreases which leads to a further increase of the mass loss rate! The model calculations allow to derive a theoretical mass loss formula for dust driven winds:

$$\dot{M}[M_\odot \mathrm{yr}^{-1}] = 10^{-3.7-0.93 M_*/M_\odot} \cdot \left(\log(\frac{L_*}{L_\odot}) - \frac{T_*}{600\mathrm{K}} \right)^{2.59 M_*/M_\odot + 1.71} \tag{66}$$

(see Dominik et al. (1990)). For more details about dust driven winds we refer to the review by Sedlmayr & Dominik (1995).

4.4 Dynamical models for dust forming shells around long–period variables

Although the stationary models are very successful for explaining the overall structure and appearance of dust forming AGB star shells and also clearly demonstrate that dust driving alone is capable of explaining the observed high mass loss rates and low outflow velocities of these objects, they of course neglect the effects introduced by the pulsation of the central stars. That these effects might be important can be inferred from several facts: i) We have seen, that a purely dust driven wind is only possible for objects having luminosities higher than the Eddington luminosity defined by Eq. (62). Observations indicate, that AGB stars with lower luminosities also produce massive, low velocity outflows. ii) Due to their evolutionary state, stars evolving along the AGB are unstable against pulsation, i.e. most objects on the AGB generally are long–period variable stars. iii) There exists a clear correlation between the infrared excess (measuring the amount of dust) and the variability of the object (Jura (1986), see Fig.19).

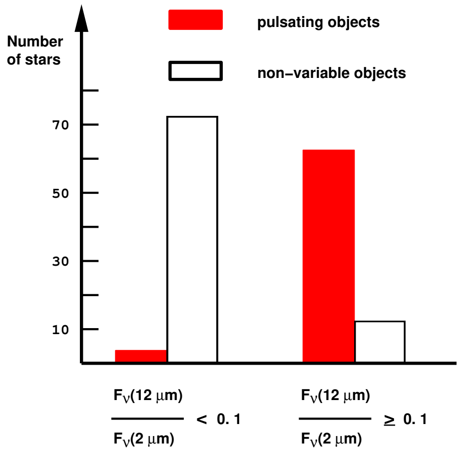

Fig. 19. Observed correlation between infrared excess and variability (after Jura (1986))

The momentum and energy input to the atmosphere by dissipation of shock waves (generated by the pulsation of the star) alone is not able to drive an outflow with the observed properties (e.g. Wood 1979). Therefore, a two step mechanism has been proposed as being responsible for the mass loss of LPVs (Jones et al. (1981)): i) levitation of the atmosphere by dissipation of shock waves and ii) subsequent acceleration of the material by radiation pressure on dust. The first consistent models for dust forming shells around LPVs have been presented by Fleischer et al. (1992). These models include a consistent, simultaneous treatment of time–dependent hydrodynamics, (equilibrium) chemistry, dust formation, growth and evaporation and of the (grey) radiative transfer problem. Since in these models only the outer regions of the star (starting inside the photosphere) are modeled, the pulsation of the star itself has to be simulated by a suitable (inner) boundary condition. This boundary condition is provided by a so–called piston approximation: The velocity at the innermost grid point is assumed to vary sinusoidally with prescribed period P and velocity amplitude Δu. Therefore, these models are described by a set of six parameters, comprising the four fundamental stellar parameters M_*, L_*, T_*, $\{\ldots, \epsilon_i, \ldots\}$ and the parameters describing the stellar pulsation P, Δu. The equations are written in Lagrangian coordinates and the calculation is started with an initially hydrostatic dust free atmosphere as initial condition (details are given in Fleischer et al. (1992)).

4.4.1 Radial shell structure of a time–dependent model Figure 20 shows the radial shell structure for a model calculation with the parameters $M_* = 1M_\odot$, $L_* = 10^4 L_\odot$, $T_* = 2600\,\mathrm{K}$, $\epsilon_\mathrm{C} = 1.80\epsilon_\mathrm{O}$ (solar abundances for the other elements), $P = 650\,\mathrm{d}$, $\Delta u = 2\,\mathrm{km\,s^{-1}}$ at a fixed instant of time. (This model is henceforth called Model A)

The following quantities are plotted: **upper diagram:** the velocity v (solid line), velocity of sound c_T (dotted line) and the temperature T (dashed line), **middle diagram:** the logarithm of the density ρ (solid line) and the degree of condensation f_c, i.e. the fraction of condensible material actually condensed into grains (dashed line) (cf. Eq. (59)), **lower diagram:** the logarithm of the nucleation rate per H–atom $J_\star/n_{<\mathrm{H}>}$, i.e. the number of dust grains formed per second and H–atom (solid line) and the logarithm of the number of dust grains per H–atom $n_\mathrm{d}/n_{<\mathrm{H}>}$ (dashed line). Radii are always given in units of the stellar radius R_0 of the initial hydrostatic model.

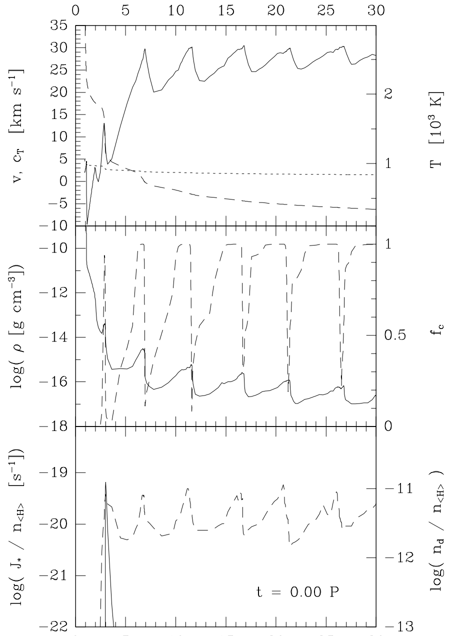

Fig. 20. Radial structure of consistent model for a pulsating, dust forming circumstellar shell

The consistent calculation of dust formation, grain growth and evaporation shows up to have significant influence on the resulting dynamic structure of the CDS.

As the degree of condensation and the number of dust grains per H–atom in Fig. 20 show, the dust is distributed inhomogeneously across the shell. The dust grains are concentrated in distinct layers and exhibit a shell or onion–like structure which is closely related to the hydrodynamic structure, e.g. the velocity profile of the CDS.

Fig. 20 also shows the determining influence of the dust on the thermodynamic structure of the CDS. There are several steps in the course of the temperature which coincide with spikes in the degree of condensation.

The discrete structure of the atmosphere is not produced solely by the shock waves caused by the interior pulsation of the star, but is a very product of the process of dust formation. In a first step the interior pulsation defines the onset of dust *formation* by providing appropriate low temperatures in the region between 3 and $4R_0$. In a second step pulsation triggers grain *growth* by a compression of the material in this radius interval and, thus, provides the high densities favorable for the growth process. In a short time interval values of f_c as high as 1 are reached, i.e. all of the condensible material is actually condensed into grains. The radiative acceleration α is directly proportional to the degree of condensation f_c (cf. Eq. (60)). Since the grains are closely momentum coupled to the gas, the sudden increase of the radiative acceleration causes a perturbation in the velocity field which steepens to become a shock wave, thereby compresses the material and, in turn, accelerates dust growth. Thus, the prominent shock waves which propagate through the atmosphere (cf. upper diagram of Fig. 20) are produced by a self–accelerating mechanism caused by the interaction between dust formation and hydrodynamics.

Furthermore, the newly formed dust in the inner shells, due to its opacity, effectively blocks the outgoing radiation and heats the material located closer to the star. This backwarming, seen as steps in the temperature structure in the upper diagram of Fig. 20, also influences the formation of new dust particles. Caused by the enhanced temperature inside the innermost dust layer, the formation of new particles is confined to a rather narrow spatial region as can be seen from the course of the nucleation rate $J_\star$ (lower diagram of Fig. 20).

Due to pulsation and backwarming, dust formation and growth is only possible in a small radius range and during a limited time interval. This results in the discrete structure of the CDS. The complex interplay among the processes of dust formation and growth, hydrodynamics and thermodynamics shows that the dust particles play the key role in determining the atmospheric structure of LPVs and Miras.

4.4.2 Temporal behavior of the models The model described in the preceding section (Model A) forms a new dust layer every piston period P. There are, however, also models, which produce new dust layers on a longer time scale, depending on the values chosen for the model parameters. This time scale is in particular sensitive to the amount of dust formed, i.e. to the carbon abundance ϵ_{C}: the lower the carbon abundance, the longer the time interval between the formation of two successive dust layers becomes. Therefore, the formation of a new dust shell can take place *every* hydrodynamic period (as in Model A), but also every second, third ... pulsational period, i.e. the radial structure of the CDS at a certain instant of time $t = \beta P$ equals the structure at $t = (\beta + n_P)P$, where β is an arbitrary dimensionless time parameter and $n_P = 1, 2, \ldots$ is the *multiperiodicity* number. (In general, n_P is not an integer number!) The formation of dust layers on time scales different from the pulsation period of the star leads to observable consequences e.g. for the light curves of these objects. As an example, Fig. 21 shows the light curves for Model A and a model calculated for the parameters $M_* = 1M_\odot$, $L_* = 3 \cdot 10^4 L_\odot$, $T_* = 2450\,\mathrm{K}$, $\epsilon_{\mathrm{C}} = 1.25\epsilon_{\mathrm{O}}$ (solar abundances for the other elements), $P = 621\,\mathrm{d}$, $\Delta u = 3\,\mathrm{km\,s^{-1}}$ (Model B).

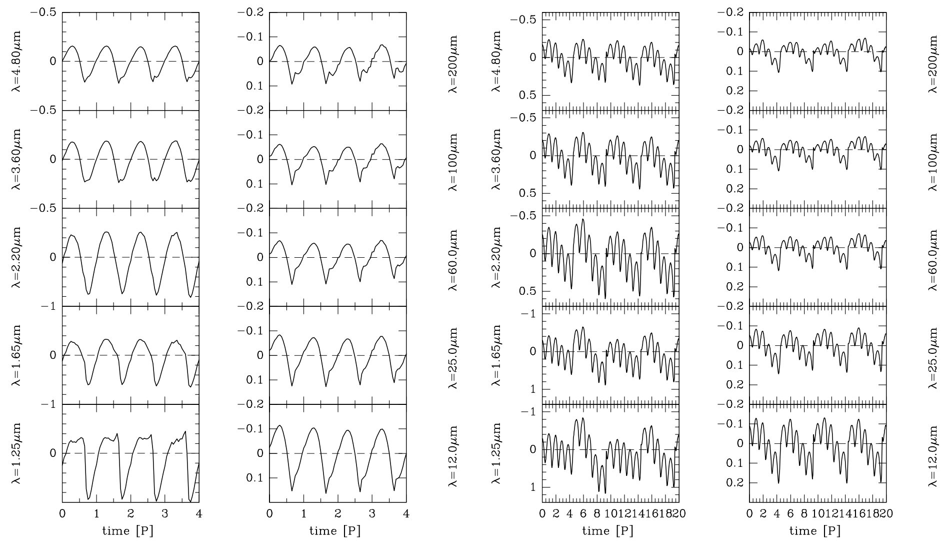

Fig. 21. Theoretical light curves (in magnitudes, relative to the mean magnitude) of Model A (l.h.s. diagrams) and Model B (r.h.s. diagrams) at different wavelengths. Note the different scaling of the ordinate at different wavelengths.

From the periodic occurrence of the different intermediate structures in Model A (l.h.s. diagram) at short wavelengths $\lambda < 2.2\mu$m and at long wavelengths $\lambda > 2.2\mu$m it can be inferred that the formation of a new dust layer periodically takes place during every second half of each hydrodynamic cycle. The light curves at wavelengths $\lambda > 2.2\mu$m show a slightly asymmetric shape and exhibit an internal structure on the rising branch which regularly occurs and is even more pronounced towards longer wavelengths. All curves are characterized by a periodic re–occurrence of all features at the same phase during the sequence of hydrodynamic pulsation cycles.

In contrast to Model A, Model B exhibits a different behavior. Model B shows a quasi–sinusoidal variation on the time scale of one pulsational period which is superposed by a long–scale oscillation on a time scale of 5 pulsation periods. In principle, the process of the formation of a new dust layer is the same in Models A and B. The difference is the time scale: The formation of a fully evolved new dust layer takes a time interval of five pulsational cycles in Model B, compared to one pulsational cycle for Model A.

A behavior similar to that produced by Models A and B has also been found in the observed light curves of real objects, e.g. for the carbon–rich objects AFGL 1085 and R For (Le Bertre 1992).

The characteristic feature of the AFGL 1085 light curves is the occurrence of intermediate extrema, already noted by Le Bertre (1992). With respect to the model calculations, these intermediate structures could be caused by the sudden formation of a new dust layer similar to Model A.

The light curves of R For show a systematic drift in magnitude very similar to the multiperiodic Model B. Secondary variations with periods multiple times longer than the main period have also been found in the light curves of several other objects by Alksnis (1990). In terms of the model calculations, this behavior could be explained by the interplay of two distinct processes with different time scales: The regular pulsation of the star, which provides the "short" hydrodynamic time scale, and the process of dust formation and growth, which, under the conditions of Model B, has a time scale five times longer. Thus, the CDS can be conceived as a dynamic system under the influence of an external excitation mechanism, or, to use a simple analogy from classical mechanics, the CDS behaves similar to a pendulum, which is subject to a periodic external force.

Irrespective of the different long–term behavior of the light curves resulting from both individual models and also independent of the different shape-variations with wavelength of the light curves of each individual model, the light amplitude decreases with increasing wavelength (cf. Fig. 21). This behavior also seems to be a general property of the real LPVs and has been noticed for many objects (see e.g. Le Bertre (1992)). In the synthetic light curves this wavelength dependence of the amplitude is largely due to the redistribution of radiative energy from short wavelengths to long wavelengths caused by the dust grains: The energy absorbed in the accessible rather narrow short wavelength portion of the stellar radiation field is redistributed by thermal dust emission over the broad infrared spectral range.

The presence of discrete dust layers in the models also causes rippled or even step–like structures in the radial brightness profiles as well as in the theoretical visibilities, which result from these calculations (see Winters et al. 1995). Similar structures have been observed e.g. for IRC +10216 by Ridgway & Keady (1988). Therefore, the discrete structure of the dust shell may provide an explanation for both, the occurrence of intermediate structures in the light curves as well as the pronounced structures in observed brightness distributions. A more detailed discussion of the observable consequences of the time–dependent model calculations can be found in Winters et al. (1994b, 1995, 1996).

5 Conclusions

We have presented the ingredients required to describe consistently the circumstellar dust shells of Red Giant stars evolving along the AGB in the HRD. An application of these considerations to the self consistent description of stationary dust driven wind situations shows that radiation pressure on dust grains alone is capable of driving a massive, low velocity outflow with the characteristic properties observed for these objects. However, this stationary wind mechanism is restricted to those objects having very high luminosities. The theoretical spectra produced by the dust shell models are in good agreement with the observations of cool carbon–rich AGB objects.

The assumption of stationarity results in the formation of rather large dust grains in the circumstellar shell. As the real dust forming objects are mostly pulsating variables, the formation of very large grains is prevented by the limitation of the time available for grain growth due to significant periodic changes of the hydrodynamic and thermodynamic conditions in the dust forming region.

Therefore, we also have presented respective consistent time–dependent model calculations, which reveal a complex interplay among the processes of dust formation and growth, hydrodynamics and thermodynamics leading to a discrete shell–like distribution of dust across the circumstellar shell. The periodic formation of these dust layers decisively influences the short–scale behavior as well as the long–term course of the light curves. The dust component plays the key role in producing features, such as intermediate extrema and secondary periods, which similarly occur in observed light curves. The layered dust distribution also causes significant time–dependent structures in the surface brightness distributions and in the synthetic visibility functions, which also are in agreement with the respective observations.

This behavior is only revealed by a consistent treatment of the complete coupled system consisting of chemistry, dust formation, hydrodynamics, thermodynamics, and radiative transfer.

Acknowledgments: We thank Dr. Cécile Loup for providing us with her tables of the CO/HCN observations in computer readable form. This work was supported by the BMBF (grant 05 3BT13A 6).

References

Alksnis A., 1990, In Mennessier M., Omont A., *From Miras to Planetary Nebulae: Which Path for Stellar Evolution?*, 279–285, Editions Frontières, Gif sur Yvette Cedex

Beck H. K. B., Gail H.-P., Henkel R., Sedlmayr E., 1992, A&A 265, 626–642

Bohren C. F., Huffman D. R., 1983, *Absorption and Scattering of Light by Small Particles*, John Wiley & Sons, New York

Danchi W. C., Bester M., Degiacomi C. G., Greenhill L. J., Townes C. H., 1994, AJ 107, 1469–1513

deJager C., Nieuwenhuijzen H., van der Hucht K. A., 1988, A&AS 72, 259–289

Dominik C., Gail H.-P., Sedlmayr E., 1989, A&A 223, 227–236

Dominik C., Gail H.-P., Sedlmayr E., Winters J. M., 1990, A&A 240, 365–375

Fleischer A. J., Gauger A., Sedlmayr E., 1992, A&A 266, 321–339

Gail H.-P., Sedlmayr E., 1987, A&A 177, 186–192

Gail H.-P., Sedlmayr E., 1988, A&A 206, 153–168

Gauger A., Gail H.-P., Sedlmayr E., 1990, A&A 235, 345–361

Goeres A., 1993, Rev. Mod. Astron. 6, 165–177

Goeres A., Henkel R., Sedlmayr E., Gail H.-P., 1988, Rev. Mod. Astron. 1, 231–248

Goeres A., Keller R., Sedlmayr E., Gail H.-P., 1996, Polycyclic Aromatic Compounds 8, 129–165

Gustafsson B., 1989, ARA&A. 27, 701–756

Holzer T. E., MacGregor K. B., 1985, In Morris M., Zuckerman B., *Mass Loss from red giants*, 229–255. D. Reidel Pub. Com.

Jones T. W., Ney E. P., Stein W. A., 1981, ApJ 250, 324–326

Jørgensen U. G., 1994, *IAU Colloquium 146: Molecules in the Stellar Environment*, Springer Verlag, Berlin

Jørgensen U. G., Johnson H. R., 1992, A&A 265, 168–176

Jura M., 1986, Irish astr. J. 17, 322–330

Keady J. J., Ridgway S. T., 1993, ApJ 406, 199–214

Knapp G. R., Morris M., 1985, ApJ 292, 640–669

Köhler T. M., Gail H.-P., Sedlmayr E., 1996, A&A in press

Le Bertre T., 1987, A&A 176, 107–113

Le Bertre T., 1992, A&AS 94, 377–398

Loup C., Forveille T., Omont A., Paul J. F., 1993, A&AS 99, 291–377

Maron N., 1990, Ap&SS 172, 21–28

Mihalas D., 1978, *Stellar Atmospheres*, W. H. Freeman and Company, San Francisco, 2^{nd} edition

Olofsson H., 1988, Space Sci. Rev. 47, 145–174

Patzer A. B. C., Köhler T., Sedlmayr E., 1995, Planet.& Sp.Sci. 43, 1233–1239

Patzer A. B. C., Winters J. M., Sedlmayr E., 1996a, In Wing R. F., *IAU Symp. 177: The Carbon Star Phenomenon*, in press, Kluwer Academic Publishers, Dordrecht

Patzer A. B. C., Gauger A., Sedlmayr E., 1996b, A&A submitted

Ridgway S. T., Keady J. J., 1988, ApJ 326, 843–858

Sahai R., Claussen M. J., Masson C. R., 1989, A&A 220, 92–98

Sedlmayr E., Dominik C., 1995, Space Sci. Rev. 73, 211–272

Sedlmayr E., Winters J. M., 1991, In Crivellari L., Hubeny I., Hummer D. G., *Stellar Atmospheres: Beyond Classical Models*, 397–408. Kluwer Academic Publishers

Tsuji T., 1986, ARA&A 24, 89–125

Walmsley C. M., Chini R., Kreysa E., Steppe H., Forveille T., Omont A., 1991, A&A 248, 555–562

Winters J. M., Dominik C., Sedlmayr E., 1994a, A&A 288, 255–272

Winters J. M., Fleischer A. J., Gauger A., Sedlmayr E., 1994b, A&A 290, 623–633

Winters J. M., Fleischer A. J., Gauger A., Sedlmayr E., 1995, A&A 302, 483–496

Winters J. M., Fleischer A. J., Le Bertre T., Sedlmayr E., 1996, A&A submitted

Witteborn F. C., Strecker D. W., Erickson E. F., Smith S. M., Goebel J. H., Taylor B. J., 1980, ApJ 238, 577–584

Wood P. R., 1979, ApJ 227, 220–231